Nuclear Receptor NR4A2 Orchestrates Th17 Cell-Mediated Autoimmune Inflammation via IL-21 Signalling

Ben J. E. Raveney, Shinji Oki[9], Takashi Yamamura*[9]

Department of Immunology, National Institute of Neuroscience, National Center of Neurology and Psychiatry, Kodaira, Tokyo, Japan

Abstract

IL-17-producing CD4+ T helper 17 (Th17) cells are pathogenic in a range of human autoimmune diseases and corresponding animal models. We now demonstrate that such T cells infiltrating the target organ during the induction of experimental autoimmune encephalomyelitis (EAE) and experimental autoimmune uveoretinitis (EAU) specifically express NR4A2. Further, we reveal a critical involvement of NR4A2 in Th17 cell functions and Th17 cell-driven autoimmune diseases. When NR4A2 expression was blocked with siRNA, full Th17 differentiation was prevented in vitro: although cells expressed the master Th17 regulator, RORγt, they expressed reduced levels of IL-23R and were unable to produce IL-17 and IL-21. Notably, Th17 differentiation in the absence of NR4A2 was restored by exogenous IL-21, indicating that NR4A2 controls full maturation of Th17 cells via autocrine IL-21 signalling. Preventing NR4A2 expression in vivo by systemic treatment with NR4A2-specific siRNA also reduced Th17 effector responses and furthermore protected mice from EAE induction. In addition, the lack of disease was associated with a reduction in autocrine IL-21 production and IL-23R expression. Similar modulation of NR4A2 expression was also effective as an intervention, reversing established autoimmune responses and ameliorating clinical disease symptoms. Thus, NR4A2 appears to control Th17 differentiation and so plays an essential role in the development of Th17-mediated autoimmune disease. As NR4A2 is also upregulated during human autoimmune disease, targeting NR4A2 may provide a new therapeutic approach in treating autoimmune disease.

Introduction

T helper (Th) cells responding to self-antigens generate pathogenic inflammatory responses in target organs, leading to local damage and so generate organ-specific autoimmune diseases. It was previously thought that CD4+ interferon (IFN)-γ-secreting Th1 cells were critical in inducing autoimmune damage to the central nervous system (CNS) in human multiple sclerosis (MS) and its animal model, experimental autoimmune encephalomyelitis (EAE) [1]. However, the discovery of pathogenic IL-17-secreting Th17 cells as a separate cell lineage opened the door to new research directions towards understanding the development of autoimmune inflammation [2–4]. It is now understood that both Th1 and Th17 cells mediate autoimmune responses in rodents [5–8] as well as in humans [9,10]. Regarding the development of EAE, it has recently been proposed that the major proportion of T cells producing inflammatory cytokines, including IFN-γ, may in fact be T cells that had previously produced IL-17 [11]. Thus, manipulation of Th17 cells might prove effective in controlling complex autoimmune disease processes involving both Th1 and Th17 cells.

Naïve CD4+ T cells differentiate into Th1 cells under the influence of IL-12, whereas TGF-β in combination with IL-6 is appreciated as the classical Th17-differentiating cytokine milieu

[12,13]. Recently, however, Th17 differentiation pathways that do not depend on IL-6 or TGF-β have also been described [14–16]. In contrast, in vivo studies demonstrate that IL-23 plays a critical role in promoting generation of Th17 cells. Indeed, Th17-mediated autoimmune disease is greatly reduced or prevented in the absence of IL-23 signalling [17,18].

NR4A2, also known as Nurr1, is an orphan nuclear receptor [19–22], and its function in dopaminergic neuron signalling has been widely known. Increasing evidence suggests the role of NR4A2 in inflammatory responses during arthritis and psoriasis [23,24], and NR4A2 may also serve as a regulatory element for reducing immune-mediated tissue damage [25]. We have previously reported that NR4A2 is among the genes expressed by circulating T cells that are highly upregulated in patients with multiple sclerosis (MS) and that NR4A2 is also induced in T cells during rodent EAE [26,27]. We also demonstrated that forced NR4A2 expression enhanced non-specific production of Th1 and Th17 cytokines although further confirmation was needed to confirm the role of NR4A2 in T cell functions.

In this study, we firstly show that NR4A2 is strikingly upregulated by IL-17-secreting Th17 cells infiltrating the target organ of EAE and experimental autoimmune uveoretinitis (EAU), the murine model of posterior uveitis. Using siRNA knockdown techniques, we demonstrate that NR4A2 is dispensable for

− 76 −

induction of the Th17 cell transcription factor RORγt in T cells, but is critically required for the *in vitro* generation of fully functional Th17 cells capable of producing IL-17 and IL-21, and expressing the IL-23 receptor (IL-23R). Notably, addition of exogenous IL-21 was able to circumvent the requirement for NR4A2 in Th17 differentiation, and restore the expression of IL-23R and IL-17. Furthermore, NR4A2 knockdown *in vivo* by injection of NR4A2 siRNA either before or after the onset of CNS infiltration ameliorated EAE. Taken together, these data suggest that T cell NR4A2 expression is a hallmark of Th17 cell-mediated pathology and show for the first time that systemic injection of a NR4A2-targeting drug may be a treatment option for Th17-cell mediated diseases.

Materials and Methods

Animals and EAE/EAU Induction

Female C57BL/6J mice (CLEA Laboratory Animal Corp., Tokyo, Japan) aged 8–10 weeks were maintained in specific pathogen–free conditions in accordance with institutional guidelines. This study and all protocols used were approval by the Committee for Small Animal Research and Animal Welfare (National Center of Neurology and Psychiatry). Procedures were carried out under institutional guidelines and all efforts were made to minimize animal suffering. For EAE induction, mice were injected subcutaneously with 100 μg MOG_{35-55} peptide (synthesized by Toray Research Center, Tokyo, Japan) and 1 mg heat-killed mycobacterium tuberculosis H37RA emulsified in complete Freund's adjuvant (Difco, KS, USA). 200 ng Pertussis toxin (List Biological Laboratories, USA) was injected intraperitoneally (*i.p.*) on days 0 and 2 after immunization. EAE was clinically scored daily (0, no clinical signs; 1, partial tail paralysis; 2, flaccid tail; 3, partial hind limb paralysis; 4, total hind limb paralysis; 5, hind and fore leg paralysis) [28]. EAU was induced as previously described by immunization with 500 μg human interphotoreceptor binding protein $(IRBP)_{1-20}$ peptide (synthesized by Toray Research Center) in CFA per mouse plus 1 μg Pertussis toxin [29]. EAU disease severity was monitored by enumeration of the retinal-infiltrating cell number as previously described [30]. Diabetes was induced as previously described [31] by 5 daily *i.p.* doses of 40 mg/kg streptozotocin (STZ; Sigma, Tokyo, Japan) and the urine glucose level was determined daily with Diastix (Bayer, Tokyo, Japan).

siRNA Treatment

NR4A2-specifc siRNA (sense – GGACAGCAGUCCUC-CAUUAAUU, anti-sense - UUAAUGGAGGACUGCUGUC-CUU) and matching scrambled control sequence siRNA were synthesized by Takara (Shiga, Japan) or Koken (Tokyo, Japan). siRNA was transfected into cells using a mouse CD4 nucleofector kit with an Amaxa electroporator (Lonza, Basel, Switzerland) according to the manufacturer's instructions. For systemic *in vivo* administration, siRNA was stabilized in atelocollagen using an AteloGene kit according to the manufacturer's instructions (Koken) and 10 μg siRNA per mouse was injected intravenously.

Cell Isolation and Purification

Single cell splenocyte and lymph node cell suspensions were generated by mechanical disruption of tissues. CNS-infiltrating lymphocytes were isolated from spinal cords and brains as previously described [28]. Briefly, tissue was cut into small pieces and digested for 40 minutes at 37°C in RPMI 1640 media (Invitrogen, Tokyo, Japan) supplemented with 1.4 mg/ml Collagenase H and 100 μg/ml DNase I (Roche, Tokyo, Japan).

Resulting tissue homogenates were forced through a 70 μm cell strainer and leukocytes were enriched using a discontinuous 37%/70% percoll density gradient centrifugation (GE Healthcare Life Sciences, Tokyo, Japan). Retinal-infiltrating cells and pancreatic-infiltrating cells were isolated by enzymatic digestion as previously described [32,33].

T cells were purified using a CD4 T cell MACS isolation kit with an AutoMACS separator according to the manufacturer's instructions (Miltenyi Biotech, Bergisch Gladbach, Germany). Where required, naïve $CD4^+CD44^-CD25^-CD62L^{high}$ T cells or memory $CD4^+CD44^+CD25^-CD62L^{low}$ T cells were further sorted using a FACS ARIA (BD Cytometry Systems, NJ, USA). For sorting of live cytokine-secreting cells, cytokine secretion assay kits (Miltenyi Biotech) were used according to the manufacturer's instructions. Briefly, cells were restimulated with 5 ng/ml PMA +500 ng/ml ionomycin (both Sigma-Aldrich, Tokyo, Japan) and anti-IL-17 and anti-IFN-γ capture antibodies were added for the final 45 minutes of culture. Secondary fluorochrome-conjugated antibodies were added to visualize captured cytokines and cells were sorted using a FACS ARIA flow cytometer.

Cell Culture

Culture media was DMEM supplemented with 10% FCS, 2 mM L-glutamine, 100 U/ml penicillin-streptomycin, and 50 μM 2-Mercaptoethanol (all Invitrogen). Where indicated, cells were activated with 2 μg/ml immobilized CD3-specific mAb (2C-11) and 1 μg/ml CD28-specific mAb (BD Pharmingen, Tokyo, Japan). Polarizing conditions were as follows: Th1, +10 ng/ml IL-12 (PeproTech, London, UK) and 10 μg/ml IL-4-specific mAb (HB188); Th17, 3 ng/ml TGF-β (R & D Systems, Minneapolis, USA), 20 ng/ml IL-6 (PeproTech), 20 ng/ml IL-23 (R & D Systems), 10 μg/ml IFN-γ-specific mAb, and 10 μg/ml IL-4-specific mAb.

Assessment of Cell Function

Cytokine concentrations in supernatants were measured by ELISA as follows: IL-17 using a mouse IL-17 DuoSet (R&D Systems), IL-21 using an IL-21 MaxLegend kit (Biolegend, San Diego, USA), and IFN-γ using a mouse IFN-γ ELISA antibody pair (BD Biosciences). Other cytokines were assessed using a FlowCytomix cytometric bead array (Bender MedSystems, Vienna, Austria) according to the manufacturer's instructions. Proliferation was determined by incubation with [³H]-thymidine (1 μCi/well) for the final 12 hours of culture and incorporation of radioactivity was assessed with a β-1205 counter (Pharmacia Biotech, Freiburg, Germany). For intracellular staining, cells were restimulated with 5 ng/ml PMA +500 ng/ml ionomycin (both Sigma-Aldrich) in the presence of Golgi Stop (BD Biosciences) for 5 hours, before surface staining and fixing/intracellular staining using a Foxp3 staining kit (eBioscience, San Diego, CA, USA) according to the manufacturer's instructions. Antibodies were sourced from BioLegend (San Diego, USA), except for anti-cytoplasmic IL-23R (Millipore, Tokyo, Japan).

RNA Extraction and Quantitative RT-PCR

Total RNA was extracted from cell populations using an RNeasy Mini Kit or FastLane kit (Qiagen, Maryland, USA) according to the manufacturer's instructions. cDNA was prepared using a first-strand cDNA Kit (Takara). Quantitative real time PCR was performed with a Light Cycler-FastStart DNA Master SYBR Green I kit using a LightCycler instrument (Roche Diagnostics, Tokyo, Japan) or with a Power SYBR green master

— 77 —

mix using an ABI 7300 real time PCR instrument (Applied Biosystems, Warrington, UK). Primers used were as follows: GAPDH, forward AACGACCCCTTCATTGAC, reverse TCCACATACTCAGCAC; RORγt, forward TGTCCTGGGCTACCCTACTG, reverse GTGCAGGAG-TAGGCCACATT; t-bet, forward GCCAGGGAACCGCTTA-TATG, reverse GACGATCATCTGGGTCACATTGT; IL-21, forward TCATCATTGACCTCGTGGCCC, reverse ATCG-TACTTCCACTTGCAATCCC; IL-23R, forward TCAGTGC-TACAATCTTCAGAGGACAT, reverse GATGGCCAAGAA-GACCATTCC; IL-17A, forward ATCCCTCAAAGCTCAGCGTGTC, reverse GGGTCTTCATTGCGGTGGAGAG; and Foxp3, forward TTCTCACAACAAGGCCACTTG, reverse CCCAGGAAAGA-CAGCAACCCT. Gene expression values were normalized to the expression of the GAPDH housekeeping gene.

Statistical Analyses

Statistical significance of differences was tested using a Mann Whitney U test unless otherwise stated. $p < 0.05$ was considered significant.

Results

Organ-specific Autoimmune Diseases EAE and EAU Accompany NR4A2 Regulation in T cells

We previously reported T cell expression of NR4A2 during EAE [27]. Here we tested whether or not NR4A2 over-expression is common to T cells involved in autoimmune diseases. We detected NR4A2 upregulation amongst T cells during the development of EAE and EAU, a Th1/Th17-mediated autoimmune disease of the retina: T cell expression of NR4A2 was observed from the earliest stages of both EAE and EAU in CD4$^+$ T cell infiltrates in the target organ and, as well as a later NR4A2 upregulation amongst circulating blood CD4$^+$ T cells (Fig. 1A&B) after the peak of clinical disease (Fig. S1A&B). Although T cells from secondary lymphoid tissue have the potential to induce EAE or EAU when they are adoptively transferred after being stimulated in vitro [34], no significant NR4A2 expression was detected amongst lymph node or splenic T cells at any time examined.

NR4A2 Expression is Associated with IL-17 Producing T cells in EAE

We previously observed that forced expression of NR4A2 in T cells could enhance production of both IL-17 and IFN-γ [27]. However, since this observation was made under non-physiological conditions, we attempted to verify if this finding had physiological meaning in vivo. Using a cytokine secretion assay, we separated populations of live CD4$^+$ T cells from the blood and CNS of EAE mice based on their production of IFN-γ and IL-17 and measured the expression levels of NR4A2 in each population. Strikingly, in the early phase of EAE, NR4A2 transcripts were detected in those T cells that produced IL-17, either alone or in combination with IFN-γ (Fig. 1C), but not in those that produced IFN-γ alone or neither IFN-γ nor IL-17. Similar findings were observed in T cells isolated from the retina during the early stages of EAU. NR4A2 expression by IL-17-secreting T cells in EAE was detected first in the target organ then later in the blood (Fig. 1D&E), which was concordant with the kinetics of NR4A2 expression in total lymphocytes (Fig. 1A).

### NR4A2 Expression is not Detected in STZ-induced Diabetes or following OVA Immunization

We next measured NR4A2 expression in T cells from streptozotocin (STZ)-induced autoimmune diabetes [35], in which autoimmune Th1 cells but not Th17 cells are thought to play a pathogenic role [31]. Repeated administration of low-dose streptozotocin (STZ) induced anti-pancreatic autoimmunity accompanied with clinical diabetes by day 10 (Fig. S1C). Consistent with a previous report [35], splenocytes as well as pancreata-infiltrating T cells produced raised levels of IFN-γ, but not IL-17, after in vitro stimulation (Fig. S1D). Unlike CNS-infiltrating T cells in EAE, NR4A2 upregulation was not detected amongst pancreata-infiltrating T cells (Fig. 1F). We also examined blood T cells from these mice and detected no NR4A2 upregulation at any time (Fig. S1E). Furthermore, we examined if NR4A2 upregulation might be induced by active immunization with any antigen in CFA. However, immunization with OVA in CFA, using the same protocol for inducing EAE with MOG peptide, did not lead to NR4A2 upregulation.

NR4A2 Expression is Required for IL-17 Production by RORγt$^+$ T cells

As NR4A2 expression appeared to be associated with IL-17-secreting pathogenic T cells, we speculated that NR4A2 might function in the process of Th17 cell differentiation. Using NR4A2-specific siRNA, we investigated in vitro if CD4$^+$ T cells differentiate normally into Th1 or Th17 cells in the absence of NR4A2 regulation. Activation of T cells leads to a rapid and transient upregulation of NR4A2 that could be prevented by transfection with NR4A2 siRNA (Fig. S2A). When NR4A2 expression was silenced in this manner, naïve CD4$^+$ T cells were able to differentiate into IFN-γ-producing cells (Fig. 2A&C), excluding a requirement for NR4A2 in Th1 cell development. However, blocking NR4A2 upregulation with siRNA greatly reduced Th17 differentiation driven by any concentrations of TGF-β, as assessed by an absence of IL-17 production (Fig. 2B&C), instead there was an increase in IFN-γ-secreting T cells. We also noted that NR4A2 knockdown did not significantly reduce the proliferation of CD4$^+$ T cells under any polarizing conditions tested (Fig. S2B), indicating that NR4A2-specific siRNA is unlikely to prevent IL-17 production by affecting cell survival. Intriguingly, despite the lack of IL-17 production in the absence of NR4A2, T cells did upregulate RORγt, the hallmark transcription factor of Th17 cells, to levels comparable to fully functional Th17 cells (Fig. 2D).

Lack of IL-17 in the Absence of NR4A2 does not Result from the Action of Foxp3

A previous study has described a failure of RORγt-expressing Th17 cells to secrete IL-17 resulting from a direct inhibitory interaction between RORγt and the transcription factor Foxp3 [36]. To examine if a similar mechanism, involving Foxp3, is applicable to interpreting our results, we measured the level of Foxp3 expression during NR4A2 knockdown. NR4A2 siRNA did not enhance but reduced Foxp3 expression in both Th17 (TGF-β+IL-6) and regulatory T cell (TGF-β alone) differentiating conditions (Fig. S3A). This finding is consistent with a recent report on a role of NR4A2 for inducing Foxp3 in regulatory T cells [37]. Furthermore, we tested if NR4A2 ablation by siRNA treatment was still effective in preventing IL-17 production when Foxp3 expression was blocked. To do this, we used Foxp3-specific siRNA to prevent Foxp3 expression in T cells that also received either control or NR4A2-specific siRNA. Foxp3 knockdown did not restore IL-17 production in the absence of NR4A2 (Fig. S3B).
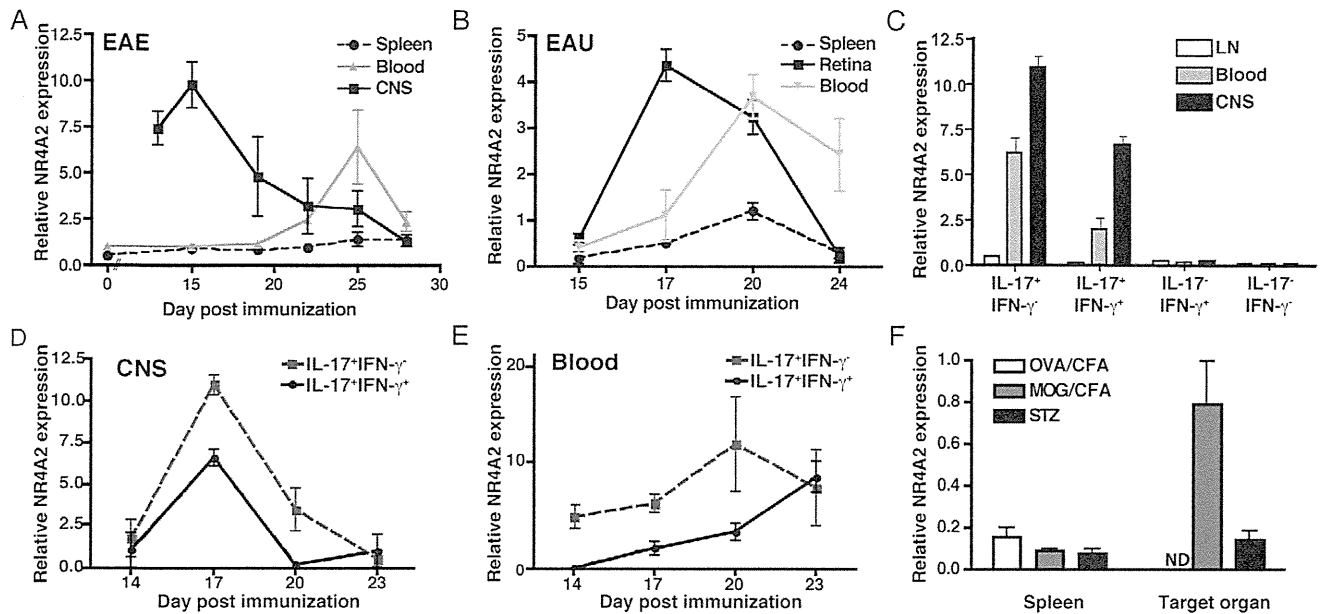
Figure 1. Autoimmune induction of NR4A2 in CD4$^+$ T cells is associated with IL-17-secreting T cells. EAE or EAU was induced in C57BL/6 mice by immunization with MOG$_{35-55}$ or IRBP$_{1-20}$ peptide in CFA, respectively. CD4$^+$ T cells were purified from spleen, blood, or target organ (CNS or retina) on the indicated days and RNA was isolated. **A** and **B:** NR4A2 expression was quantified by real time PCR relative to GAPDH for T cells from EAE (A) or EAU (B). Timepoints correspond to a minimum of 5 animals and data are representative of 3 independent experiments. CD4$^+$ T cells from mice with EAE were restimulated with PMA/ionomycin for 3 hours and 4 populations of cytokine secreting cells (IL-17+IFN-γ-, IL-17+IFN-γ+, IL-17-IFN-γ+, and IL-17-IFN-γ-) were sorted by flow cytometry using IFN-γ and IL-17 cytokine secretion assay kits. **C:** NR4A2 expression by populations of cytokine-secreting CD4$^+$ T cells was quantified by real time PCR at day 15 post-EAE induction for lymph nodes (LN) and CNS-infiltrating cells (CNS), and day 25 for blood T cells. **D** and **E:** NR4A2 expression by IL-17$^+$IFN-γ$^-$ or IL-17$^+$IFN-γ$^+$ CNS-infiltrating T cells (D) or blood T cells (E) was measured by real time PCR at a range of timepoints. Data are representative of 2 independent experiments. **F:** Th1-mediated diabetes was induced in C57BL/6 mice by 5 daily low dose STZ treatments. Other groups of C57BL/6 mice were immunized with peptides in CFA plus PTX either OVA$_{323-339}$ (OVA/CFA) or MOG$_{35-55}$ (MOG/CFA). On day 22, NR4A2 expression was assessed by real time PCR amongst CD4$^+$ T cells from spleen and leukocytes isolated from the relevant target organ (ND, OVA/CFA; CNS, EAE; pancreas, STZ). Timepoints correspond to a minimum of 5 animals and data are representative of 2 independent experiments.
doi:10.1371/journal.pone.0056595.g001

Thus, NR4A2 appears to be required for IL-17 production by Th17 cells, and the underlying mechanism is independent of RORγt and Foxp3.

NR4A2 Controls the IL-21-initiated Phase of Th17 Differentiation

RORγt expression is required for generation of fully functional Th17 cells. However, when upregulation of NR4A2 is prevented, Th17-polarized RORγt$^+$ T cells do not acquire the ability to produce IL-17 (Fig. 2). A possible scenario is that RORγt regulation is an early event in Th17 differentiation [38], whereas later induction of NR4A2 is critical for inducing signals that promote IL-17 production. IL-21-deficient or IL-21R-deficient T cells resemble NR4A2-deficient T cells in that they express RORγt but do not produce IL-17 under Th17 polarizing condition [4,39]. Thus, we suspected that NR4A2 expression might control IL-17 production via autocrine IL-21 signalling. IL-21 is produced during early Th17 cell differentiation and then acts in an autocrine manner to induce IL-23R upregulation by Th17 cells [38,40]; the subsequent action of IL-23 produced by myeloid cells then enhances and stabilizes the Th17 cell phenotype via IL-23R. To clarify the kinetics of these key molecules, we evaluated the expression of IL-21, IL-23R, and IL-17 transcripts by RORγt$^+$ T cells during in vitro Th17 cell differentiation. IL-21 begins to be produced before IL-23R is upregulated, which itself precedes IL-17 expression (Fig. 3A). Interestingly, NR4A2 siRNA transfection strongly inhibited the sequential regulation of IL-21, IL-23R, and

IL-17 RNA transcripts (Fig. 3A). We also confirmed the reduction of IL-21 by NR4A2 siRNA treatment at the protein level (Fig. 3B). These data indicate that NR4A2 may be required for IL-21 production and thus in turn control Th17 differentiation. Furthermore, the lack of NR4A2 also blocked c-maf upregulation (Fig. 3C), a transcription factor reported to control IL-21 expression in Th17 development [41]. Finally, Th17 differentiation yields normal IL-22 production in the absence of NR4A2 (Fig. 3D) and the generation of IL-22 has been shown to be related to pathways downstream of RORγt, but independent of c-maf, IL-21, and IL-23 signalling [42]. To test the hypothesis that NR4A2 is required for full Th17 differentiation due to its role in the c-maf/IL-21/IL-23R pathway, we reintroduced this pathway by adding exogenous IL-21 to cultures. Critically, the presence of exogenous IL-21 restored IL-17 secretion by T cells stimulated under Th17 polarizing conditions despite the lack of NR4A2 (Fig. 4A). Additionally, NR4A2-knocked down Th17 cells cultured with IL-21 also expressed equivalent levels of IL-23R to the control Th17 cells (Fig. 4B).

NR4A2 Controls the Severity of EAE

Next we tested if NR4A2 also controlled pathogenic Th17 responses in EAE. Administration of NR4A2-specific siRNA on the day of EAE induction was effective at preventing NR4A2 expression by CNS-infiltrating T cells (Fig. S4A). Such systemic blockade of NR4A2 suppressed the onset of clinical EAE (Fig. 5A), accompanied by a reduced ability of CNS-infiltrating CD4$^+$ T

– 79 –
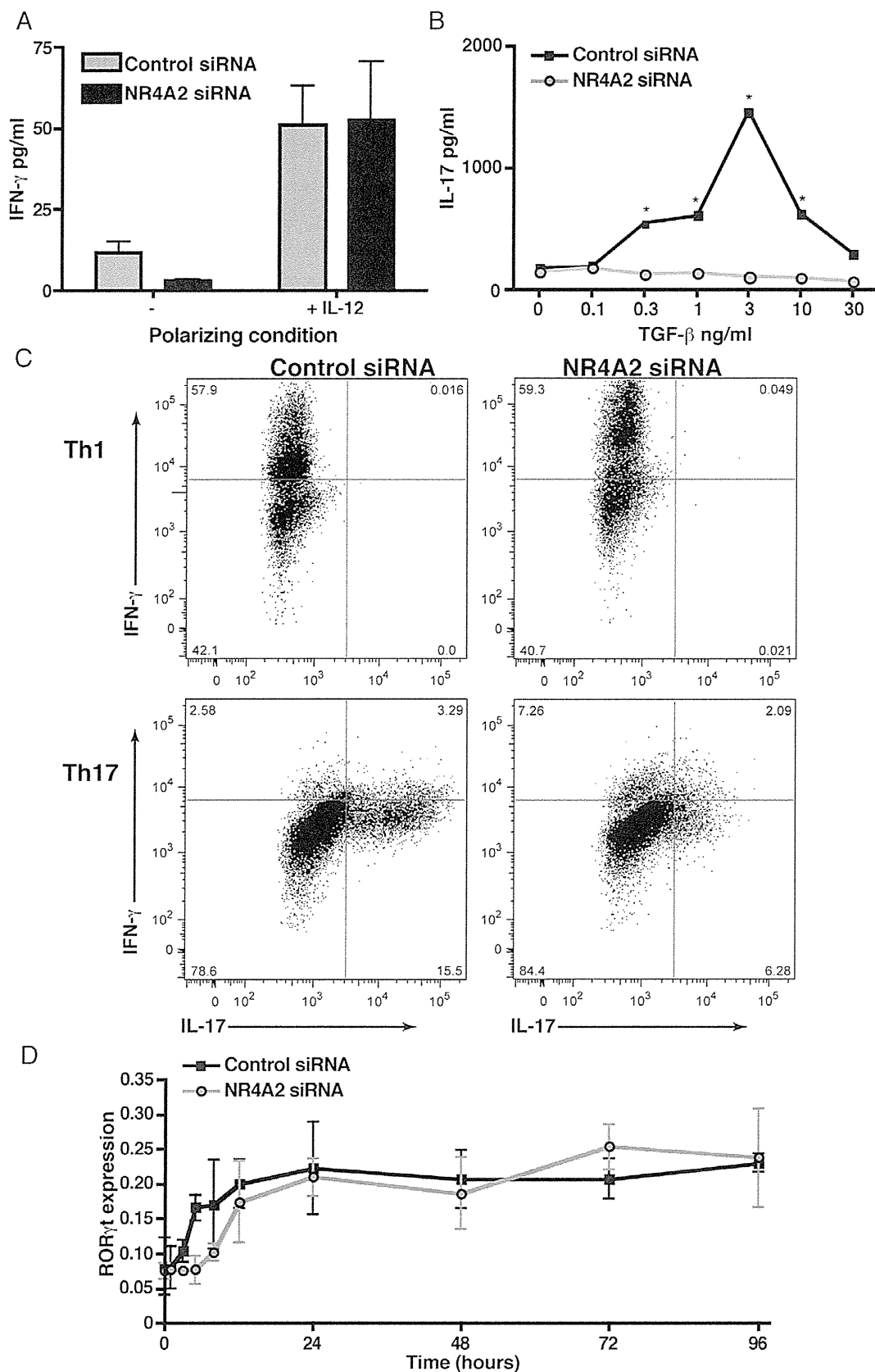
Figure 2. NR4A2 knockdown prevents IL-17 secretion but not RORγt upregulation. Naïve CD4^{+} T cells were transfected by electroporation with NR4A2-specific siRNA or scrambled control siRNA. Cells were then activated with 5 µg/ml plate-bound CD3-specific mAb and 0.5 µg/ml soluble CD28-specific mAb. **A:** IFN-γ production by cells activated in the presence or absence of 10 ng/ml IL-12 after 96 hours of culture. **B:** IL-17 production

by cells activated in the presence of 20 ng/ml IL-6, 20 ng/ml IL-23, and TGF-β at a range of concentrations after 96 hours of culture. Significant differences between control and NR4A2 siRNA-treatments were tested with a student's t-test, *p<0.05. **C:** IL-17 and IFN-γ intracellular cytokine staining for transfected T cells (control siRNA, left plots; NR4A2 siRNA, right plots) cultured for 96 hours in the presence of 10 ng/ml IL-12 (Th1 conditions, top row plots) or 20 ng/ml IL-6, 20 ng/ml IL-23, and 3 ng/ml TGF-β (Th17 conditions, bottom row plots). **D:** RORγt RNA expression as measured by real time PCR by activated T cells cultured under Th17 polarizing conditions at a range of timepoints. Data are representative of 5 independent experiments.
doi:10.1371/journal.pone.0056595.g002

cells to secrete IL-17 but not IFN-γ (Fig. 5B) when restimulated with the immunizing peptide. NR4A2 siRNA treatment also led to a lower proportion of T cells in the target organ that produced IL-17 upon non-specific restimulation during early timepoints (summarized in Fig. 5C; representative data, Fig. S4B). However,

we observed that the effect of NR4A2 siRNA is not persistent, and the mice showed signs of late onset EAE after day 21 (Fig. 5A) accompanied by an increase in the proportion of IL-17^{+} T cells in the CNS (Fig. 5C). Since collagen-stabilized siRNA maintains its suppressive activity *in vivo* for approximately three weeks [43], the
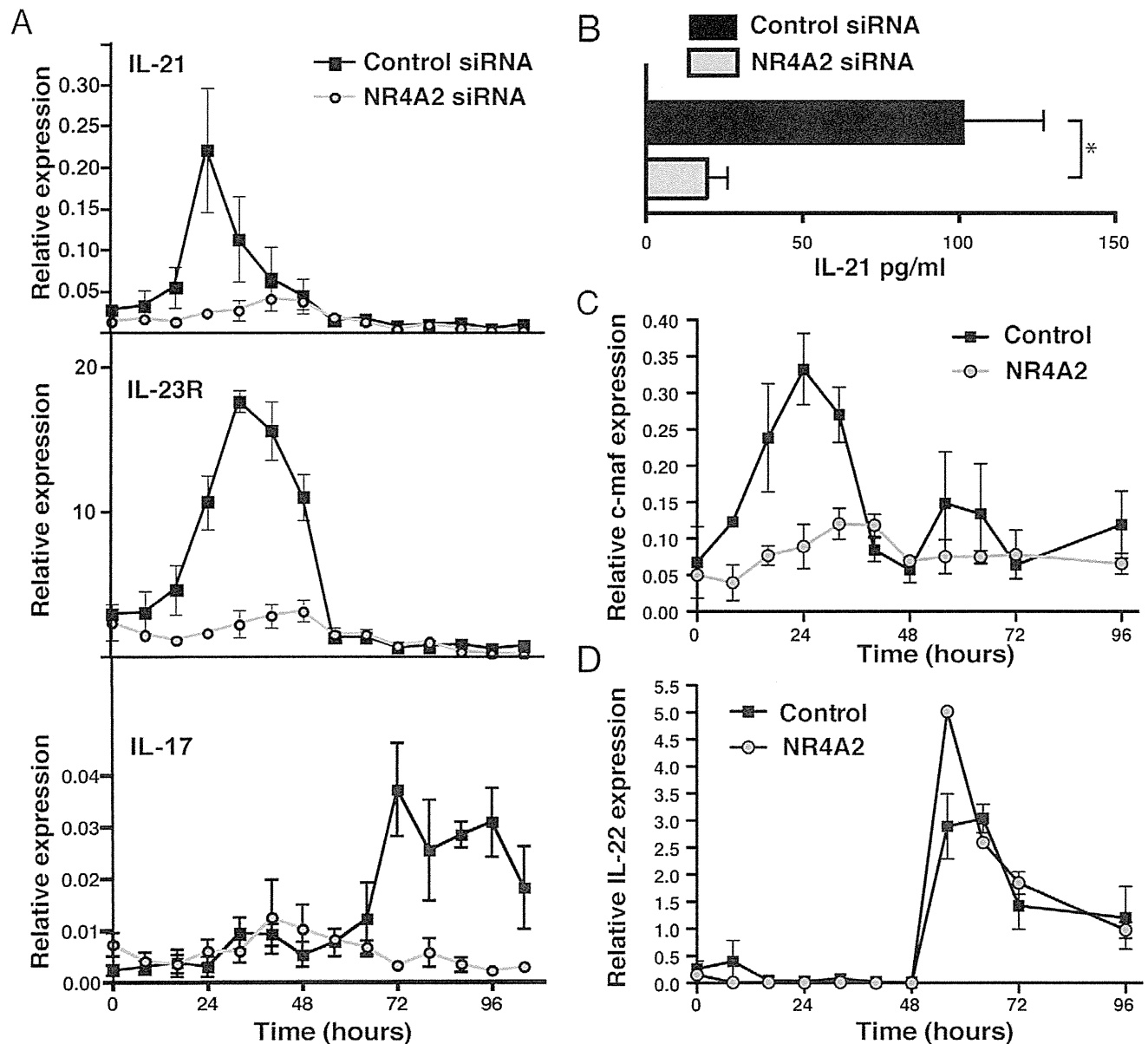
Figure 3. Absence of NR4A2 is associated with a lack of IL-21 production by Th17 cells. Naïve CD4^{+} T cells were transfected by electroporation with NR4A2-specific siRNA or scrambled control siRNA and were activated with 5 μg/ml plate-bound CD3-specific mAb and 0.5 μg/ml soluble CD28-specific mAb in the presence of 20 ng/ml IL-6, 20 ng/ml IL-23, and 3 ng/ml TGF-β. **A:** RNA levels of IL-21, IL-23R, and IL-17 were quantified by real time PCR at the indicated timepoints following activation. Data are representative of 3 independent experiments. **B:** IL-21 supernatant concentration was measured by ELISA at 96 hours. Data are representative of 3 independent experiments. *p<0.05. **C:** RNA expression of c-maf quantified by real time PCR. **D:** RNA expression of IL-22 quantified by real time PCR. Data are representative of 2 independent experiments.
doi:10.1371/journal.pone.0056595.g003

— 81 —
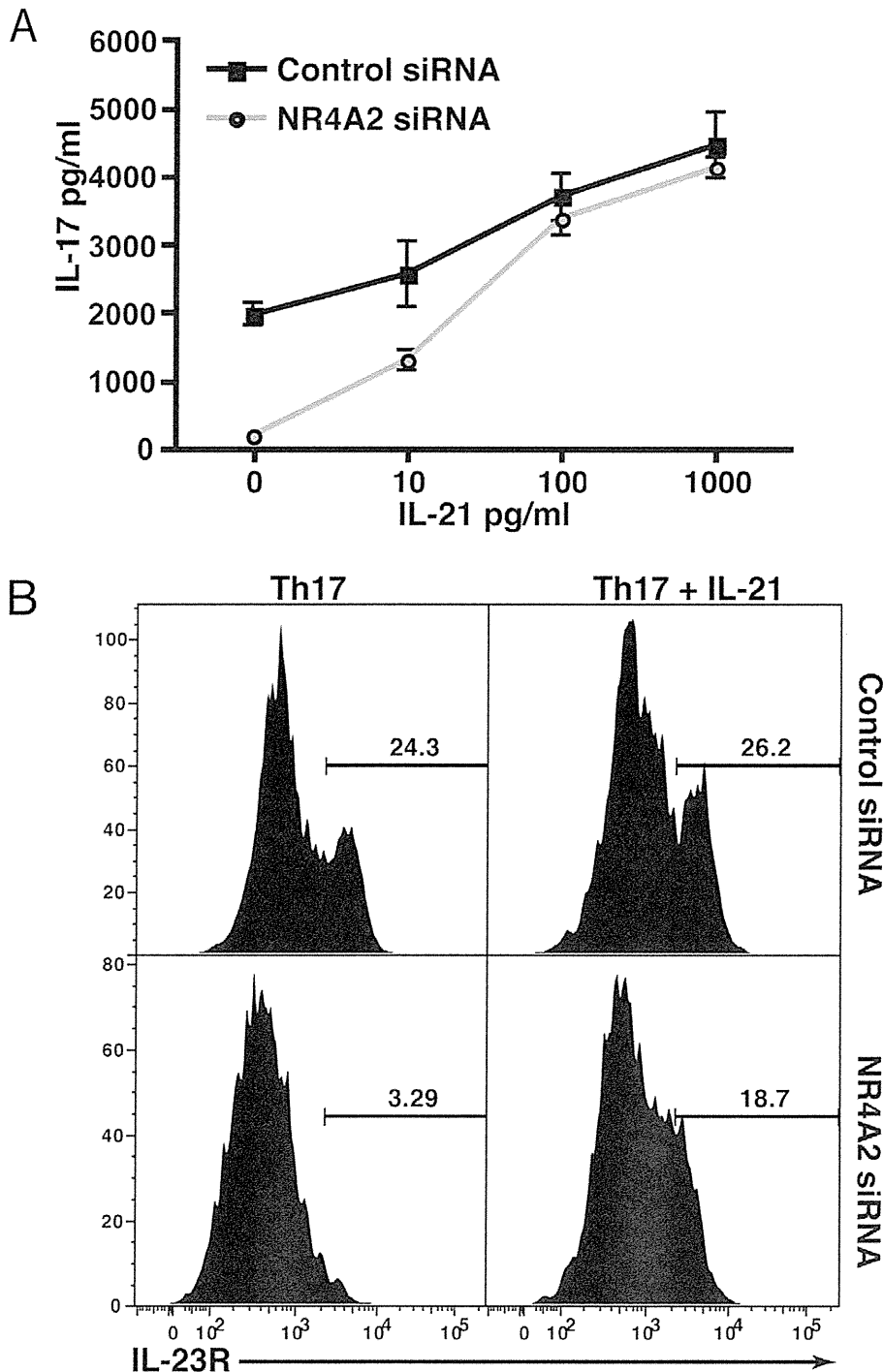
Figure 4. Exogenous IL-21 restores IL-17 production in the absence of NR4A2. Naïve CD4+ T cells were transfected by electroporation with NR4A2-specific siRNA or scrambled control siRNA and were activated with 5 µg/ml plate-bound CD3-specific mAb and 0. 5 µg/ml soluble CD28-specific mAb in the presence of 20 ng/ml IL-6, 20 ng/ml IL-23, and 3 ng/ml TGF-β. To some wells, recombinant IL-21 was added as indicated. **A:** IL-17 was measured in the supernatants of control or NR4A2 siRNA-treated T cells by ELISA after 96 hours of culture under Th17 polarizing conditions in the presence or absence of IL-21 at the indicated concentrations. *p<0.05. Data are representative of 3 independent experiments. **B:** IL-23R expression was assessed by intracellular flow cytometric staining after 96 hours of culture under Th17 polarizing conditions in the presence (right plots) or absence (left plots) of 100 pg/ml recombinant IL-21 for control siRNA-treated T cells (top) and NR4A2 siRNA-treated T cells (bottom row). Data are representative of 2 independent experiments.
doi:10.1371/journal.pone.0056595.g004

later onset of EAE may reflect the reduced potency of the siRNA. We then tested the effect of injection of NR4A2 siRNA at a later timepoint. Interestingly, when the NR4A2 siRNA was given on

day 10 post-EAE induction, clinical EAE was greatly reduced, and unlike treatment at day 0, no increase in disease was observed after day 20 (Fig. 5D). These results indicate that NR4A2 targeting

— 82 —

siRNA is not only preventative, but also therapeutic against the development of EAE. Furthermore, the CNS-infiltrating T cells also showed reduced expression of IL-21 and IL-23R (Fig. 5E&F), reminiscent of the *in vitro* blocking of NR4A2 during Th17 cell differentiation. Based on these data, we suggest that NR4A2 is a key factor for Th17 differentiation *in vivo* during the initiation of autoimmune responses via its control of IL-21 and IL-23R expression.

Discussion

In this study, we demonstrate that the orphan nuclear receptor NR4A2 is highly expressed by IL-17-secreting T cells infiltrating the target organ of EAE and EAU. When upregulation of NR4A2 was prevented *in vitro*, Th17-polarizing T cells expressing RORγt did not further differentiate into mature Th17 cell capable of producing IL-21 and IL-17. This inhibition of Th17 cell differentiation was associated with disruption of autocrine IL-21 signalling. *In vitro* analysis showed that adding exogenous IL-21 restored the ability of the NR4A2 knocked-down Th17 cells to express IL-23R and produce IL-17. Furthermore, *in vivo* injection of NR4A2 siRNA prevented the development of EAE by specifically inhibiting Th17 cell production of IL-17, but not affecting Th1 cells. Based on these findings, we propose that NR4A2 has direct effects on T cell pathogenicity or plays a critical role in continuous new Th17 differentiation and thus it orchestrates effector functions of Th17 cells in mediating autoimmune diseases.

Reagents that dampen the function of Th17 cells are of practical interest in clinical settings. Indeed, an IL-17A-specific antibody was efficacious in clinical trials of human psoriasis, uveitis, and rheumatoid arthritis [44]. Although the effects of IL-17 blockade on EAE appear to be only modest [45,46], clinical trials are currently in progress to test IL-17A-specific antibody treatment in MS patients. As Th17 cells probably generate a range of proinflammatory cytokines, it is debatable how effective a therapy targeting a single cytokine may prove. NR4A2 appears to control various molecules regulated by IL-21 signalling and therefore a drug targeting NR4A2 may prove more effective than an antibody against a single cytokine.

We previously described that forced expression of NR4A2 in resting T cells led to a modest increase in IFN-γ production following nonspecific stimulation and suggested that NR4A2 might be involved in both Th1 and Th17 cell responses [27]. In contrast, we here reveal that only Th17 cells were found to express NR4A2 in the lesions of EAE, implying that NR4A2 plays a more important role in Th17 cells than in Th1 cells during autoimmune inflammation. However, it is not surprising to see a reduced IFN-γ production in NR4A2 knocked-down T cells *in vitro* (Fig. 2A), since IL-21 has potentials to modulate IFN-γ production under particular conditions [47]. An unexpected report was that the absence of NR4A2 led to increased expression of IFN-γ [37]. The authors argued that the increased production of IFN-γ was due to reduced activity of Foxp3^{+} regulatory T cells that are also dependent on NR4A2 [37]. However, this report does not contradict with our results, because in our *in vitro* experiments, we have explicitly removed regulatory T cells from the starting cell populations.

In agreement with previous studies [17,48], our results showed that autocrine IL-21 production would promote IL-23R expression and subsequent production of IL-17 during Th17 cell
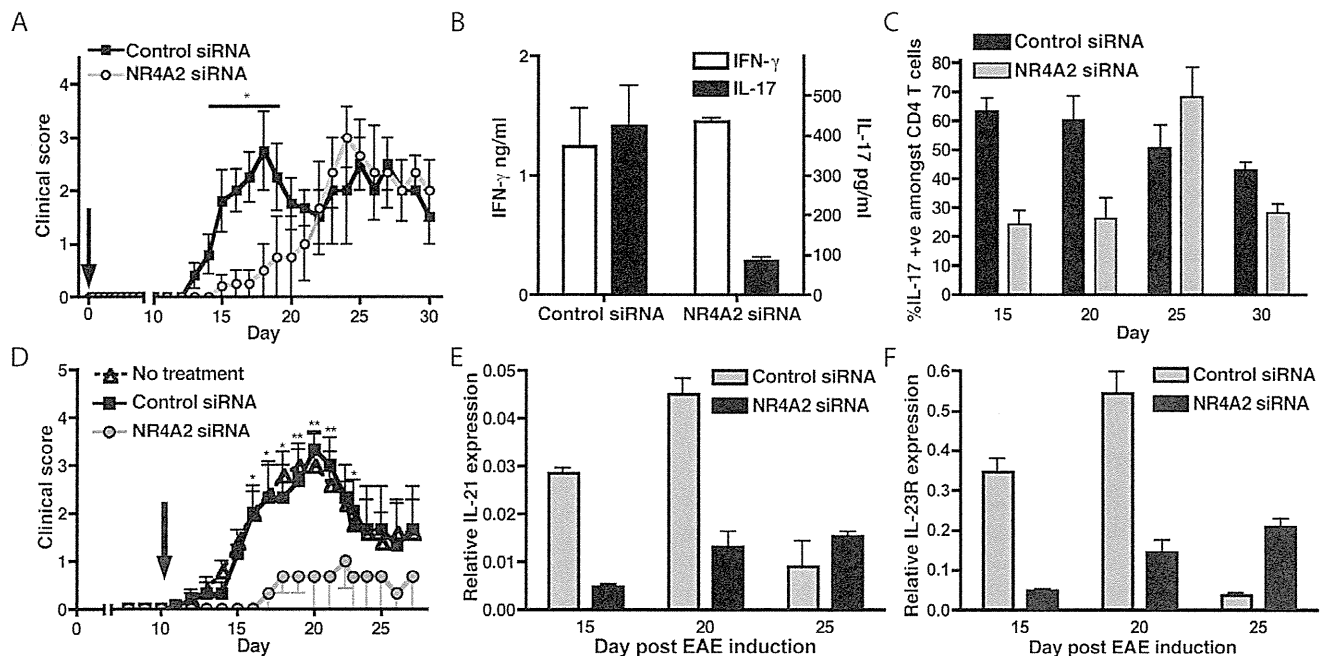
Figure 5. Systemic administration of NR4A2-specific siRNA reduces EAE severity. siRNA, either NR4A2-specific or control, was stabilized in a collagen matrix and administered *i.v.* to groups of C57BL/6 mice at the time of EAE induction. EAE was scored clinically (**A**) and at day 15 post-EAE induction, production of IL-17 and IFN-γ by CNS-infiltrating leukocytes restimulated with 20 μg/ml MOG peptide for 96 hours were assessed by ELISA (**B**). CNS-infiltrating T cells were also assessed for IL-17 production at a range of timepoints by intracellular flow cytometry (**C**). Data are representative of 3 independent experiments. Control or NR4A2-specific siRNA was applied to MOG-immunized mice at day 10 post-disease induction and disease was scored clinically (**D**). Timepoints correspond to a minimum of 5 animals and data are representative of 2 independent experiments. IL-21 and IL-23R expressions amongst CNS-infiltrating T cells were measured by real time PCR (**E&F**). Data are representative of 2 independent experiments. Clinical scores in panels A) and D) were tested with a two-way ANOVA test. *p<0.01, **p<0.001.
doi:10.1371/journal.pone.0056595.g005

differentiation. When NR4A2 upregulation was blocked by siRNA treatment, the production of IL-17 was greatly reduced, although RORγt expression was maintained, but exogenously added IL-21 restored IL-17 and IL-23R expression. Furthermore, NR4A2 also appeared to be required for the induction of the transcription factor that controls IL-21 secretion following Th17 differentiation, c-maf [41]. Moreover, lack of NR4A2 had little effect on RORγt expression, implying that this transcription factor is not associated with an IL-21-related pathway. It is interesting that IL-22 production is also maintained in the absence of NR4A2, despite the lack of IL-23R, suggesting that this cytokine could be produced via IL-23-independent pathways. TGF-β signals usually inhibit IL-22 production [16], however it is conceivable that these inhibitory signals are ineffective without NR4A2, thus allowing IL-22 secretion in the absence of increased IL-23R expression. Thus, NR4A2 modulation of Th17 cells may be limited to a role in the c-maf/IL-21 pathway, which ultimately controls IL-23R regulation and subsequent signalling. Given the critical role of IL-23 during pathogenic Th17 cell differentiation [16], the ability of NR4A2 siRNA to affect IL-23R expression by inhibiting IL-21 production cannot be ignored. It has been shown that IL-21 can drive Th17 differentiation [49] and thus enhance the initiation phase of EAE [50]. Therefore, the NR4A2-IL-21 pathway is particularly interesting as a therapeutic target. On the other hand, although a report claims that IL-21 is essential for Th17 differentiation [39], other reports showed Th17 differentiation in the absence of IL-21, albeit at a reduced level [14], and IL-17 production and EAE induction were not entirely blocked without IL-21 autocrine signals [51,52]. The discrepancy regarding the role of IL-21 in Th17 cell induction remains to be fully understood and it is possible that absence of IL-21 signalling in gene knockout mice may be compensated by an alternative cytokine signalling pathway. However, our data may be explained by direct effects of NR4A2 on IL-23R upregulation as well as on the c-maf/IL-21 pathway.

In conclusion, our findings highlight the application of siRNA *in vivo* to modulate immunologic pathways that generate pathogenic autoimmune responses. Furthermore, our discovery of the key role of NR4A2 signalling in Th17 differentiation and our identification of the involvement of NR4A2 in generating autoimmune response *in vivo* suggest a new target for intervention in Th17-mediated autoimmune disease. This view is supported by our direct demonstration that manipulation of NR4A2 expression by siRNA treatment in established disease ameliorated clinical symptoms. Thus, future therapies targeting NR4A2 may prove highly effective in treating particular autoimmune diseases.

Supporting Information

Figure S1 EAE or EAU was induced in C57BL/6 mice by immunization with MOG$_{35-55}$ or IRBP$_{1-20}$ peptide in CFA. EAE was scored clinically (A). CD4$^+$ T cells were purified from the retina on the indicated days, and EAU disease severity was evaluated by flow cytometric enumeration of ocular infiltrates for EAU (B). Timepoints correspond to a minimum of 5 animals and data are representative of 3 independent experiments. A group of C57BL/6 mice received a low dose of STZ daily for 5 days. Clinical diabetes was tested by measurement of urine glucose level, with diabetes confirmed by consecutive urine glucose result of greater than ≥300 mg/dl (C). Plot C shows percentage diabetes. Other groups of C57BL/6 mice were immunized with peptides in CFA plus PTX either OVA$_{323-339}$ (OVA/CFA) or MOG$_{35-55}$ (MOG/CFA). On day 22, splenocytes and leukocytes isolated from the relevant target organ (ND, OVA/CFA; CNS,

EAE; pancreas, STZ) were restimulated with 20 mg/ml of the immunizing peptide, or with soluble anti-CD3 (for STZ); after 96 hours, IL-17 and IFN-γ were measured in supernatants by ELISA (D). NR4A2 expression by blood T cells was also measured at a range of timepoints (E). Timepoints correspond to a minimum of 5 animals and data are representative of 2 independent experiments.
(TIF)

Figure S2 Naïve CD4$^+$ T cells were transfected by electroporation with NR4A2-specific siRNA or scrambled control siRNA. Cells were then activated with 5 µg/ml plate-bound CD3-specific mAb and 0.5 µg/ml soluble CD28-specific mAb in the presence of 20 ng/ml IL-6, 20 ng/ml IL-23, and 3 ng/ml TGF-β. NR4A2 expression was assessed at a range of timepoints by RT PCR (A). Data are representative of 5 independent experiments. Cell proliferation of transfected cells following anti-CD3/anti-CD28 stimulation in the presence of Th1 (+10 ng/ml IL-12), Th17 (+20 ng/ml IL-6, 20 ng/ml IL-23, and 3 ng/ml TGF-β), or in the absence of polarizing cytokines was measured at 96 hours by the incorporation of ^{3}H-thymidine. Data are representative of 2 independent experiments.
(TIF)

Figure S3 Naïve CD4$^+$ T cells transfected by electroporation with NR4A2-specific siRNA or scrambled control siRNA were activated with plate-bound CD3-specific mAb and soluble CD28-specific mAb in the presence of 10 µg/ml IFN-γ-specific and IL-4-specific mAb, with either 20 ng/ml IL-6, 2 ng/ml TGF-β (IL-6+ TGF-β) or with 10 ng/ml TGF-β (TGF-β). Foxp3 expression at 96 hours as measured by real time PCR is shown in plot A. Data shown represent averages of 4 independent experiments. Naïve CD4$^+$ T cells were transfected by electroporation with 2 siRNAs: either Foxp3-specific siRNA or relevant scrambled control siRNA and with either NR4A2-specific siRNA or relevant scrambled control siRNA. This yielded 4 cell types: 1) Foxp3 control/NR4A2 control (C/C); 2) Foxp3 control/NR4A2 siRNA (C/N); 3) Foxp3 siRNA/NR4A2 control (F/C); and 4) Foxp3 siRNA/NR4A2 siRNA (F/N). Cells were then activated with plate-bound CD3-specific mAb and soluble CD28-specific mAb in the presence of 10 µg/ml IFN-γ-specific and IL-4-specific mAb with either 20 ng/ml IL-6, 2 ng/ml TGF-β (IL-6+ TGF-β) or with 10 ng/ml TGF-β (TGF-β). Plot B shows IL-17 production from each of 4 siRNA-treated cell types at 96 hours as measured by ELISA. Data are representative of 2 independent experiments. siRNA, either NR4A2-specific or control, was stabilized in a collagen matrix and administered *i.v.* to groups of C57BL/6 mice at the time of EAE induction. At the indicated timepoints, CNS-infiltrating T cells were FACS-sorted and NR4A2 expression was assessed by RT PCR (A). CNS-infiltrating leukocytes from day 15 post-EAE induction from control or NR4A2 siRNA-treated mice were restimulated with PMA/ionomycin for 5 hours, and IL-17 and IFN-γ production were visualized by intracellular flow cytometric staining (B). Data are representative of 3 independent experiments
(TIF)

Figure S4 siRNA, either NR4A2-specific or control, was stabilized in a collagen matrix and administered *i.v.* to groups of C57BL/6 mice at the time of EAE induction. At the indicated timepoints, CNS-infiltrating T cells were FACS-sorted and NR4A2 expression was assessed by RT PCR (A). CNS-infiltrating leukocytes from day 15 post-EAE induction from control or NR4A2 siRNA-treated mice were restimulated with PMA/ionomycin for 5 hours, and IL-17 and IFN-γ production

— 84 —

were visualized by intracellular flow cytometric staining (B). Data are representative of 3 independent experiments. (TIF)

References

1. Sospedra M, Martin R (2005) Immunology of multiple sclerosis. Annu Rev Immunol 23: 683–747.
2. Bettelli E, Korn T, Kuchroo VK (2007) Th17: the third member of the effector T cell trilogy. Curr Opin Immunol 19: 652–657.
3. Damsker JM, Hansen AM, Caspi RR (2010) Th1 and Th17 cells: adversaries and collaborators. Ann N Y Acad Sci 1183: 211–221.
4. Korn T, Oukka M, Kuchroo V, Bettelli E (2007) Th17 cells: effector T cells with inflammatory properties. Semin Immunol 19: 362–371.
5. Goverman J (2009) Autoimmune T cell responses in the central nervous system. Nat Rev Immunol 9: 393–407.
6. Jager A, Dardalhon V, Sobel RA, Bettelli E, Kuchroo VK (2009) Th1, Th17, and Th9 effector cells induce experimental autoimmune encephalomyelitis with different pathological phenotypes. J Immunol 183: 7169–7177.
7. Luger D, Silver PB, Tang J, Cua D, Chen Z, et al. (2008) Either a Th17 or a Th1 effector response can drive autoimmunity: conditions of disease induction affect dominant effector category. J Exp Med 205: 799–810.
8. Steinman L (2008) A rush to judgment on Th17. J Exp Med 205: 1517–1522.
9. Man S, Ubogu EE, Ransohoff RM (2007) Inflammatory cell migration into the central nervous system: a few new twists on an old tale. Brain Pathol 17: 243–250.
10. Matusevicius D, Kivisakk P, He B, Kostulas N, Ozenci V, et al. (1999) Interleukin-17 mRNA expression in blood and CSF mononuclear cells is augmented in multiple sclerosis. Mult Scler 5: 101–104.
11. Hirota K, Duarte JH, Veldhoen M, Hornsby E, Li Y, et al. (2011) Fate mapping of IL-17-producing T cells in inflammatory responses. Nat Immunol 12: 255–263.
12. Bettelli E, Carrier Y, Gao W, Korn T, Strom TB, et al. (2006) Reciprocal developmental pathways for the generation of pathogenic effector TH17 and regulatory T cells. Nature 441: 235–238.
13. Korn T, Bettelli E, Oukka M, Kuchroo VK (2009) IL-17 and Th17 Cells. Annu Rev Immunol 27: 485–517.
14. Korn T, Bettelli E, Gao W, Awasthi A, Jager A, et al. (2007) IL-21 initiates an alternative pathway to induce proinflammatory T(H)17 cells. Nature 448: 484–487.
15. Das J, Ren G, Zhang L, Roberts AI, Zhao X, et al. (2009) Transforming growth factor beta is dispensable for the molecular orchestration of Th17 cell differentiation. J Exp Med 206: 2407–2416.
16. Ghoreschi K, Laurence A, Yang XP, Tato CM, McGeachy MJ, et al. (2011) Generation of pathogenic T(H)17 cells in the absence of TGF-beta signalling. Nature 467: 967–971.
17. Cua DJ, Sherlock J, Chen Y, Murphy CA, Joyce B, et al. (2003) Interleukin-23 rather than interleukin-12 is the critical cytokine for autoimmune inflammation of the brain. Nature 421: 744–748.
18. McGeachy MJ, Cua DJ (2007) The link between IL-23 and Th17 cell-mediated immune pathologies. Semin Immunol 19: 372–376.
19. Law SW, Conneely OM, DeMayo FJ, O'Malley BW (1992) Identification of a new brain-specific transcription factor, NURR1. Mol Endocrinol 6: 2129–2135.
20. Perlmann T, Wallen-Mackenzie A (2004) Nurr1, an orphan nuclear receptor with essential functions in developing dopamine cells. Cell Tissue Res 318: 45–52.
21. Le WD, Xu P, Jankovic J, Jiang H, Appel SH, et al. (2003) Mutations in NR4A2 associated with familial Parkinson disease. Nat Genet 33: 85–89.
22. Pearen MA, Muscat GE (2010) Minireview: Nuclear Hormone Receptor 4A Signaling: Implications for Metabolic Disease. Mol Endocrinol 24: 1–13.
23. Aherne CM, McMorrow J, Kane D, FitzGerald O, Mix KS, et al. (2009) Identification of NR4A2 as a transcriptional activator of IL-8 expression in human inflammatory arthritis. Mol Immunol 46: 3345–3357.
24. O'Kane M, Markham T, McEvoy AN, Fearon U, Veale DJ, et al. (2008) Increased expression of the orphan nuclear receptor NURR1 in psoriasis and modulation following TNF-alpha inhibition. J Invest Dermatol 128: 300–310.
25. Saijo K, Winner B, Carson CT, Collier JG, Boyer L, et al. (2009) A Nurr1/CoREST pathway in microglia and astrocytes protects dopaminergic neurons from inflammation-induced death. Cell 137: 47–59.
26. Satoh J, Nakanishi M, Koike F, Miyake S, Yamamoto T, et al. (2005) Microarray analysis identifies an aberrant expression of apoptosis and DNA damage-regulatory genes in multiple sclerosis. Neurobiol Dis 18: 537–550.
27. Doi Y, Oki S, Ozawa T, Hohjoh H, Miyake S, et al. (2008) Orphan nuclear receptor NR4A2 expressed in T cells from multiple sclerosis mediates production of inflammatory cytokines. Proc Natl Acad Sci U S A 105: 8381–8386.
28. Klemann C, Raveney BJ, Klemann AK, Ozawa T, von Horsten S, et al. (2009) Synthetic retinoid AM80 inhibits Th17 cells and ameliorates experimental autoimmune encephalomyelitis. Am J Pathol 174: 2234–2245.
29. Raveney BJ, Copland DA, Nicholson LB, Dick AD (2008) Fingolimod (FTY720) as an acute rescue therapy for intraocular inflammatory disease. Arch Ophthalmol 126: 1390–1395.
30. Copland DA, Wertheim MS, Armitage WJ, Nicholson LB, Raveney BJ, et al. (2008) The clinical time-course of experimental autoimmune uveoretinitis using topical endoscopic fundal imaging with histologic and cellular infiltrate correlation. Invest Ophthalmol Vis Sci 49: 5458–5465.
31. Mensah-Brown EP, Shahin A, Al-Shamisi M, Wei X, Lukic ML (2006) IL-23 leads to diabetes induction after subdiabetogenic treatment with multiple low doses of streptozotocin. Eur J Immunol 36: 216–223.
32. Fraser JM, Janicki CN, Raveney BJ, Morgan DJ (2006) Abortive activation precedes functional deletion of CD8+ T cells following encounter with self-antigens expressed by resting B cells in vivo. Immunology 119: 126–133.
33. Raveney BJ, Copland DA, Dick AD, Nicholson LB (2009) TNFR1-dependent regulation of myeloid cell function in experimental autoimmune uveoretinitis. J Immunol 183: 2321–2329.
34. Shao H, Liao T, Ke Y, Shi H, Kaplan HJ, et al. (2006) Severe chronic experimental autoimmune uveitis (EAU) of the C57BL/6 mouse induced by adoptive transfer of IRBP1-20-specific T cells. Exp Eye Res 82: 323–331.
35. Elias D, Prigozin H, Polak N, Rapoport M, Lohse AW, et al. (1994) Autoimmune diabetes induced by the beta-cell toxin STZ. Immunity to the 60-kDa heat shock protein and to insulin. Diabetes 43: 992–998.
36. Zhou L, Lopes JE, Chong MM, Ivanov, II, Min R, et al. (2008) TGF-beta-induced Foxp3 inhibits T(H)17 cell differentiation by antagonizing RORgammat function. Nature 453: 236–240.
37. Sekiya T, Kashiwagi I, Inoue N, Morita R, Hori S, et al. (2011) The nuclear orphan receptor Nr4a2 induces Foxp3 and regulates differentiation of CD4+ T cells. Nat Commun 2: 269.
38. Zhou L, Ivanov, II, Spolski R, Min R, Shenderov K, et al. (2007) IL-6 programs T(H)-17 cell differentiation by promoting sequential engagement of the IL-21 and IL-23 pathways. Nat Immunol 8: 967–974.
39. Nurieva R, Yang XO, Martinez G, Zhang Y, Panopoulos AD, et al. (2007) Essential autocrine regulation by IL-21 in the generation of inflammatory T cells. Nature 448: 480–483.
40. Ivanov, II, Zhou L, Littman DR (2007) Transcriptional regulation of Th17 cell differentiation. Semin Immunol 19: 409–417.
41. Bauquet AT, Jin H, Paterson AM, Mitsdoerffer M, Ho IC, et al. (2009) The costimulatory molecule ICOS regulates the expression of c-Maf and IL-21 in the development of follicular T helper cells and TH-17 cells. Nat Immunol 10: 167–175.
42. Veldhoen M, Hirota K, Westendorf AM, Buer J, Dumoutier L, et al. (2008) The aryl hydrocarbon receptor links TH17-cell-mediated autoimmunity to environmental toxins. Nature 453: 106–109.
43. Takeshita F, Minakuchi Y, Nagahara S, Honma K, Sasaki H, et al. (2005) Efficient delivery of small interfering RNA to bone-metastatic tumors by using atelocollagen in vivo. Proc Natl Acad Sci U S A 102: 12177–12182.
44. Hueber W, Patel DD, Dryja T, Wright AM, Koroleva I, et al. (2011) Effects of AIN457, a fully human antibody to interleukin-17A, on psoriasis, rheumatoid arthritis, and uveitis. Sci Transl Med 2: 52ra72.
45. Hofstetter HH, Ibrahim SM, Koczan D, Kruse N, Weishaupt A, et al. (2005) Therapeutic efficacy of IL-17 neutralization in murine experimental autoimmune encephalomyelitis. Cell Immunol 237: 123–130.
46. Komiyama Y, Nakae S, Matsuki T, Nambu A, Ishigame H, et al. (2006) IL-17 plays an important role in the development of experimental autoimmune encephalomyelitis. J Immunol 177: 566–573.
47. Monteleone G, Monteleone I, Fina D, Vavassori P, Del Vecchio Blanco G, et al. (2005) Interleukin-21 enhances T-helper cell type I signaling and interferon-gamma production in Crohn's disease. Gastroenterology 128: 687–694.
48. Langrish CL, Chen Y, Blumenschein WM, Mattson J, Basham B, et al. (2005) IL-23 drives a pathogenic T cell population that induces autoimmune inflammation. J Exp Med 201: 233–240.
49. Leonard WJ, Spolski R (2005) Interleukin-21: a modulator of lymphoid proliferation, apoptosis and differentiation. Nat Rev Immunol 5: 688–698.
50. Vollmer TL, Liu R, Price M, Rhodes S, La Cava A, et al. (2005) Differential effects of IL-21 during initiation and progression of autoimmunity against neuroantigen. J Immunol 174: 2696–2701.
51. Coquet JM, Chakravarti S, Smyth MJ, Godfrey DI (2008) Cutting edge: IL-21 is not essential for Th17 differentiation or experimental autoimmune encephalomyelitis. J Immunol 180: 7097–7101.
52. Sonderegger I, Kisielow J, Meier R, King C, Kopf M (2008) IL-21 and IL-21R are not required for development of Th17 cells and autoimmunity in vivo. Eur J Immunol 38: 1833–1838.

Author Contributions

Conceived and designed the experiments: BR SO TY. Performed the experiments: BR. Analyzed the data: BR SO. Wrote the paper: BR SO TY.

— 85 —

Research Report

Multimodal image analysis of sensorimotor gating in healthy women

Miho Ota[a],*, Noriko Sato[b], Junko Matsuo[a], Yukiko Kinoshita[a], Yumiko Kawamoto[a], Hiroaki Hori[a], Toshiya Teraishi[a], Daimei Sasayama[a], Kotaro Hattori[a], Satoko Obu[a], Yasuhiro Nakata[b], Hiroshi Kunugi[a]

[a]Department of Mental Disorder Research, National Institute of Neuroscience, National Center of Neurology and Psychiatry, 4-1-1 Ogawa-Higashi, Kodaira, Tokyo 187–8502, Japan
[b]Department of Radiology, National Center of Neurology and Psychiatry, 4-1-1 Ogawa-Higashi, Kodaira, Tokyo 187-8551, Japan

ARTICLE INFO

ABSTRACT

Prepulse inhibition (PPI) deficits have been reported in individuals with schizophrenia and other psychiatric disorders with dysfunction of the cortico–striato–pallido–thalamic circuit. The purpose of this study was to investigate the structural neural correlates of PPI by using magnetic resonance imaging (MRI) metrics. The subjects were 53 healthy women (mean age; 40.7 ± 11.3 years). We examined the possible relationships between PPI and diffusion tensor imaging (DTI) metrics to estimate white matter integrity and gray matter volume analyzed using the DARTEL (diffeomorphic anatomical registration through exponentiated lie) algebra method. There were significant correlations between DTI metrics and PPI in the parahippocampal region, the anterior limb of the internal capsule, the ventral tegmental area, the thalamus and anterior thalamic radiations, the left prefrontal region, the callosal commissural fiber, and various white matter regions. There were also positive correlations between PPI and gray matter volume in the bilateral parietal gyri and the left inferior prefrontal gyrus at a trend level. The present study revealed evidence of a relationship between PPI and the integrity of white matter. This result was compatible with the previous suggestion that PPI would be modulated by the cortico-striato-thalamic-pallido-pontine circuit.

© 2013 Elsevier B.V. All rights reserved.

1.   Introduction

The startle reflex can be attenuated when the startling stimulus is preceded by a weak non-startling prepulse, in a process called prepulse inhibition (PPI). The degree to which such a prepulse inhibits the startle reflex in PPI is used as a measure of sensorimotor gating. Disruptions in information processing and attention have long been thought of as one of the hallmarks of schizophrenia (McGhie and Chapman, 1961), and PPI has been suggested as a neurophysiologic measure of information processing abnormalities in schizophrenia (Cadenhead and Braff, 1999).

There is evidence from animal studies that PPI is modulated by forebrain circuits involving the prefrontal cortex, thalamus, hippocampus, amygdala, nucleus accumbens, striatum, and globus pallidus (Koch and Schnitzler, 1997; Swerdlow and Geyer, 1998; Swerdlow et al., 2001). Deficient PPI is observed in several neuropsychiatric disorders characterised by abnormalities in the cortico-striato-thalamic-pontine circuitry (Braff et al., 2001; Swerdlow et al., 2008). Previous neuroimaging studies using structural brain images revealed the neural correlates of PPI in the prefrontal and orbitofrontal cortex, hippocampus extending to the parahippocampal gyrus, the basal ganglia including parts of putamen, the globus pallidus, and the nucleus accumbens, posterior cingulate, superior temporal gyrus, and thalamus (Kumari et al., 2005, 2008a). Several functional magnetic resonance imaging (fMRI) studies showed that PPI is associated with increased bilateral activation in the striatum extending to the hippocampus, insula, thalamus, and inferior frontal, middle temporal, and inferior parietal lobes (Hazlett et al., 2001, 2008; Kumari et al., 2003, 2008a). A regression analysis demonstrated a linear relationship between PPI and blood oxygenation level-dependent (BOLD) activity in the thalamus, nucleus accumbens, and inferior parietal region (Kumari et al., 2003). Positron emission tomography (PET) study also detected an association between PPI and the prefrontal and inferior parietal cortices' glucose metabolism

(Hazlett et al., 1998). Although it is known that PPI disruption resulted from the interruption of the cortico–striato–thalamic–pontine neural circuit, to our knowledge there has been no study verifying the integrity of white matter using diffusion tensor imaging (DTI).

The present study was conducted to investigate the structural basis of PPI deficits using DTI and volumetry analysis. We hypothesized that PPI would be correlated with components in the hippocampus/temporal lobe, basal ganglia, cingulate gyrus, and frontal and parietal regions.

2.   Results

Initially, we examined the correlation between the gray matter volume and % PPI using DARTEL (diffeomorphic anatomical registration using exponentiated lie). There was no significant correlation between them; however, there were nominal trends between % PPI with 90 dB prepulse and gray matter volume in the bilateral parietal gyri and left inferior prefrontal regions ($p < 0.005$ uncorrected) (Fig. 1(A)), and between % PPI with 86 dB prepulse and gray matter volume in the left parietal and medial frontal regions ($p < 0.005$ uncorrected) (Fig. 1(B)).

We then examined correlation between % PPI and DTI. Significant positive correlations were observed between fractional anisotropy (FA) value and % PPI with 90 dB prepulse in the right ventral tegmental area, left anterior limbs of the internal capsule, bilateral thalami, and the left inferior prefrontal region, bilateral medial frontal regions, and bilateral parietal regions ($p < 0.001$ uncorrected) (Fig. 2(A) to (F)), however, we could detect correlation between % PPI with 86 dB prepulse and FA values only in the inferior prefrontal region (Fig. 2(G)) ($p < 0.001$ uncorrected). In addition, analysis using the skeletonized FA data showed that there were significant positive correlations between FA value and % PPI with 90 dB prepulse in the parahippocampal region, orbitofrontal region, bilateral temporal–inferior parietal regions, internal capsule,
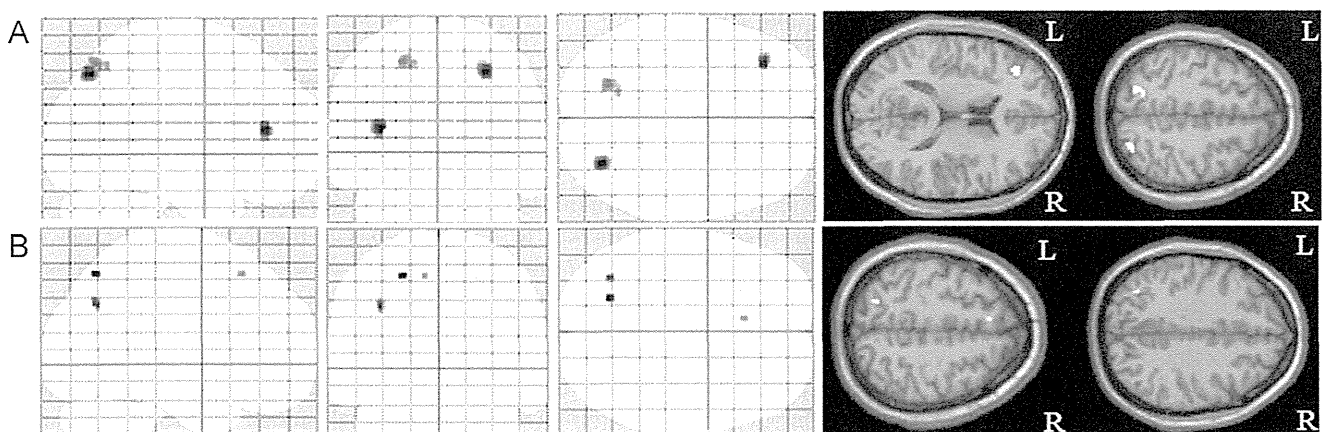
Fig. 1 – Brain areas in which % PPI and gray matter volume showed correlation. There was no significant correlation between % PPI and gray matter volume. However, a nominal trend was found in the bilateral parietal regions and left inferior prefrontal regions (A) ($p < 0.005$ uncorrected). Likewise, there was a nominal correlation between % PPI with 86 dB prepulse and gray matter volume in the left parietal and medial frontal regions (B) ($p < 0.005$ uncorrected). Age and whole brain volume were controlled. L, left; R, right.
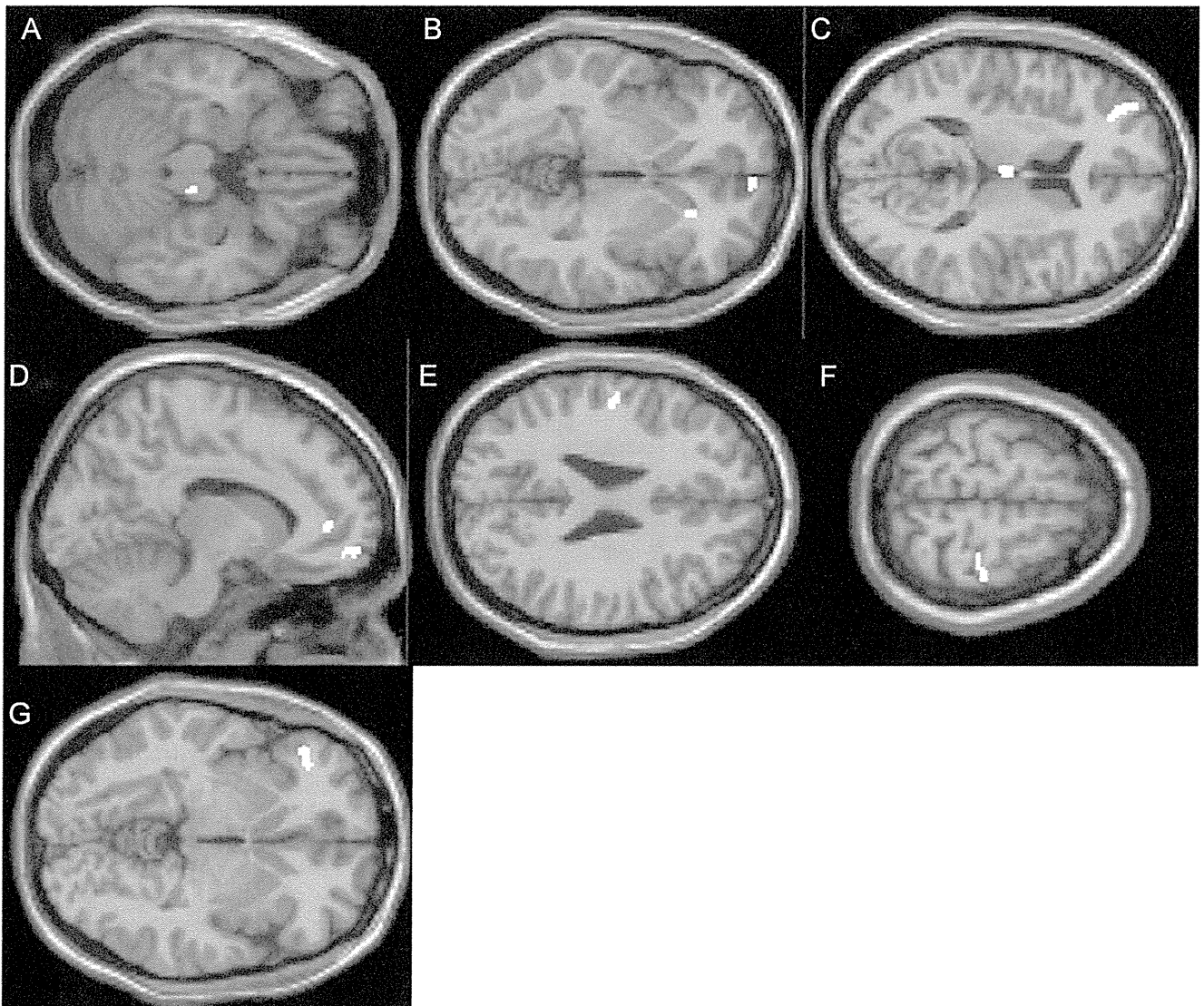
Fig. 2 – Brain areas in which % PPI and FA values correlated. There were positive correlations between % PPI with 90 dB of prepulse and FA values in the right ventral tegmental area (A), left anterior limbs of internal capsule (B), bilateral thalami, and left inferior prefrontal region (C), bilateral medial frontal regions ((B), (D)), and bilateral parietal regions ((E) and (F)) ($p < 0.001$ uncorrected). Correlation between % PPI with 86 dB of prepulse and FA values was seen only in the inferior prefrontal region (G) ($p < 0.001$ uncorrected). Age was controlled. L, left; R, right.
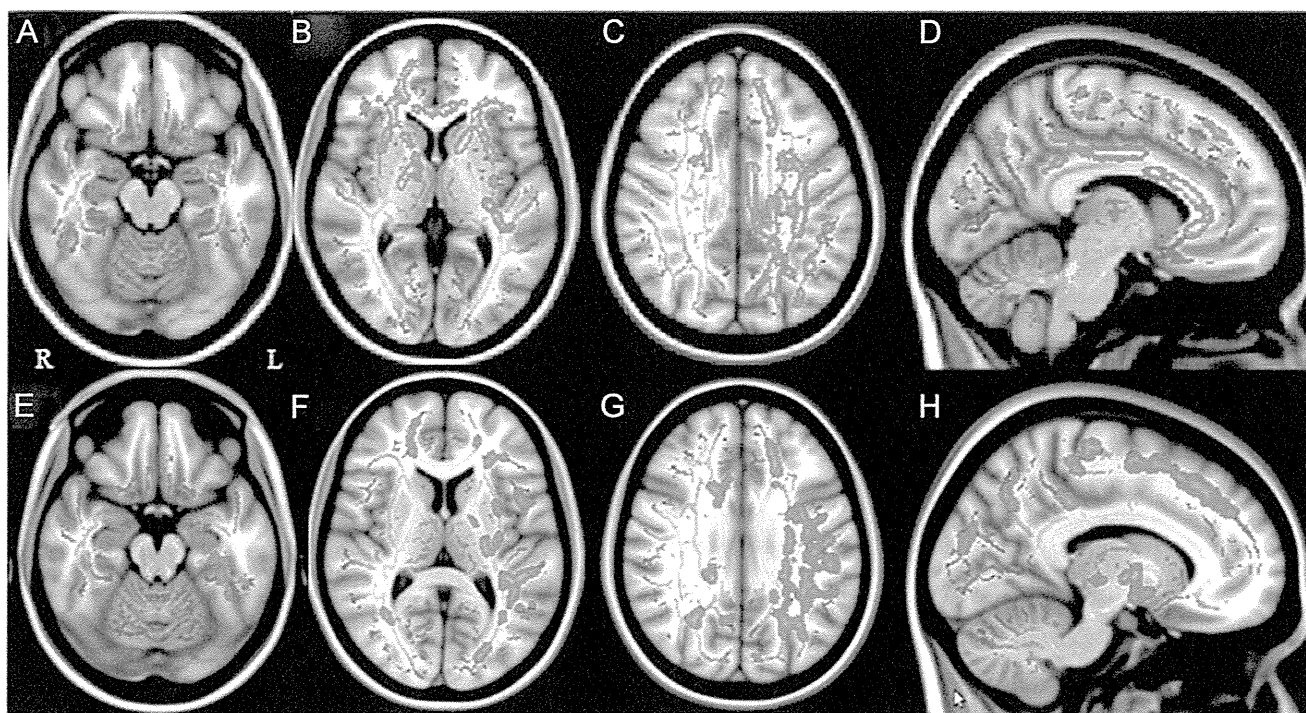
thalamus, anterior thalamic radiations, posterior cingulate, and callosal commissural fibers ($p < 0.05$, family-wise error (FWE) rate is controlled) (Fig. 3(A) to (D)). On the other hand, there were no significant correlation between % PPI with 86 dB prepulse and FA value, and only nominal trends were revealed in similar regions (Fig. 3(E) to (H)) ($p < 0.1$; FWE rate is controlled).

There were significantly positive correlations between % PPI and the mean diffusivity (MD) values in many regions throughout the brain (90 dB; Fig. 4(A), 86 dB; Fig. 4(B)). To be more conservative, we corrected for multiple testing by false discovery rate (FDR) and set the critical p-value as < 0.01(90 dB), and by FWE and set the critical p-value as < 0.05 (86 dB). After this procedure, the correlations of PPI with MD values in the left inferior prefrontal region remained significant (Fig. 4(A) and (B), the right column).

3. Discussion

To our knowledge, this is the first study that used DTI to examine the possible relationships between PPI and brain structure in healthy subjects. Significant correlations were noted between PPI and DTI metrics in the ventral tegmental area, parahippocampus, callosal commissural fiber, thalamus, anterior thalamic radiation, internal capsule, posterior cingulate, and temporal and parietal regions. There were nominal trends between PPI and gray matter volume in the left inferior prefrontal region and bilateral parietal regions. Our results are consistent with previous neuroimaging studies using structural MRI and fMRI and pharmacological studies (Hazlett et al., 2001; Kumari et al., 2005; Swerdlow et al., 2001).

Consistent with the consensus regarding PPI in the rat, a number of psychiatric and neurological disorders characterized

Fig. 3 – Brain areas in which % PPI and FA values correlated using TBSS. There were positive correlations between % PPI with 90 dB of prepulse and FA values in the parahippocampal region (A), orbitofrontal region (A), temporal–parietal regions ((B) and (C)), internal capsules (B), thalamus and anterior thalamic radiations ((B) and (C)), posterior cingulate ((C) and (D)), and anterior dominant callosal commissural fibers ((B) and (D)) revealed by tract-based spatial statistics (TBSS) ($p < 0.05$; family-wise error rate is controlled). On the other hand, there were no significant correlations between % PPI with 86 dB of prepulse and FA values, however, a nominal trend was detected in similar regions ((E) to (H)) ($p < 0.1$; family-wise error rate is controlled). Age was controlled. The skeleton, shown in green, is thresholded at 0.2 and overlaid onto the MNI152 space. L, left; R, right. (For interpretation of the references to colour in this figure legend, the reader is referred to the web version of this article.)
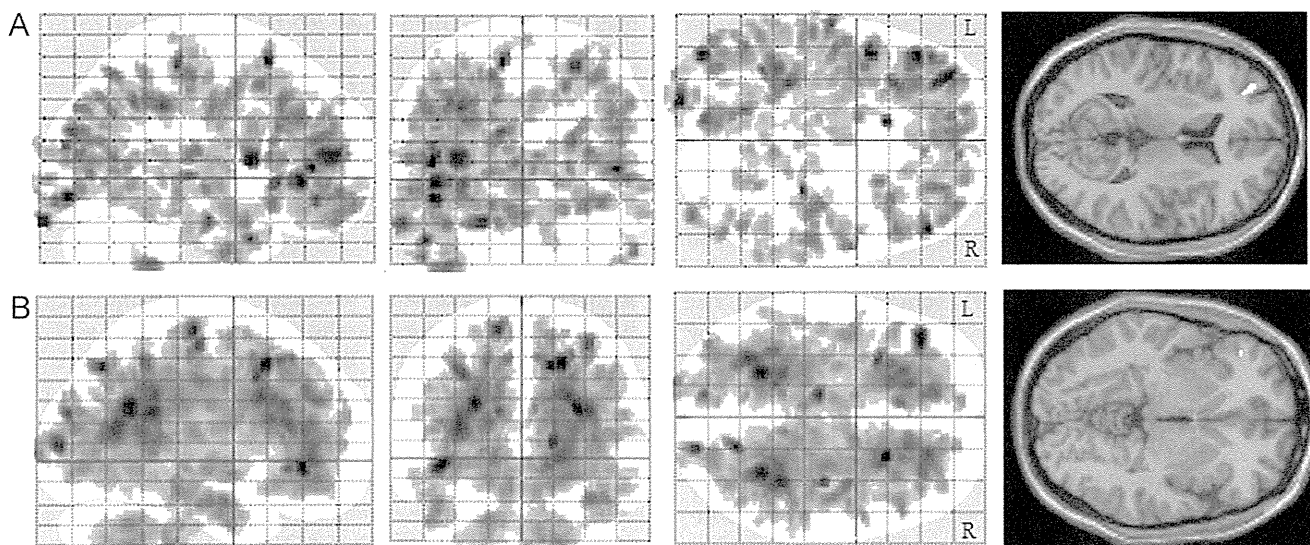
Fig. 4 – Brain areas in which % PPI and MD values correlated. There were negative correlations between % PPI with 90 (A) and 86 dB (B) of prepulse and MD values in several areas throughout the brain ($p < 0.001$ uncorrected). The right column showed that the correlations remained when we re-analyzed the correlation between PPI and MD values in the left inferior prefrontal region (90 dB; $p < 0.01$ [false discovery rate], 86 dB; $p < 0.05$ [family-wise error rate]). L, left; R, right.

by abnormalities at some level in the cortico–striato–thalamic–pontine circuitry (Braff et al., 2001; Swerdlow et al., 2008) and in the cortico–striato–pallido–thalamic brain substrate (Perry et al., 2004; Swerdlow et al., 2008) showed the PPI deficient. Previous neuroimaging studies revealed the correlation between PPI and regional brain using structural brain images (Kumari et al., 2005,

2008b), and fMRI (Hazlett et al., 2001, 2008; Kumari et al., 2003, 2007, 2008a). Here we found significant correlations between PPI and DTI metrics in the parahippocampus, the internal capsule, the circumference of anterior thalamic radiation and the parietal region. In light of these observations, PPI may be regulated through an amygdala – basal ganglia – prefrontal and parietal circuit. There is evidence from animal studies that PPI is mediated by brain stem circuits involving the inferior colliculus, superior colliculus, pedunculopontine tegmental nucleus, laterodorsal tegmental nucleus, substantia nigra pars reticulata, and caudal pontine reticular nucleus (Fendt et al., 2001). In the present study, we detected a correlation between FA in the ventral tegmental area and % PPI, a finding that is compatible with this previous evidence.

As described above, previous studies showed that PPI is influenced by many regions throughout the brain, and PPI is thought to be affected by the transmission of information. We therefore hypothesized that to evaluate the relation between PPI and the brain, the use of DTI – which shows the condition of the neural fibers – would be effective. Our DTI results suggested that a large area of the brain is involved in deficits in PPI, compared to the foregoing studies focusing on the gray matter. This may be due to the ability of DTI to delineate neural pathways. Furthermore, we detected more correlations between % PPI and brain metrics when prepulse was 90 dB than when it was 86 dB. Previous studies showed that % PPI at the prepulse intensity of 90 dB was higher compared with that at 86 dB, and that the difference in % PPI between patients with schizophrenia and healthy controls became most significant when prepulse was 90 dB (Kunugi et al., 2007; Takahashi et al., 2008; Moriwaki et al., 2009). These points may suggest that % PPI with 90 dB of prepulse is the best condition to reflect his/her own information processing and attention.

Regarding the volumetric analysis, we could not detect any significant relationship between the PPI and gray matter volume, although the data showed a nominal trend of a relationship in the inferior frontal gyrus and bilateral parietal regions. As to the association between the inferior prefrontal region and PPI, we detected this relationship by all metrics used in this study. This connection was previously detected in an MRI volumetric study (Kumari et al., 2005). However, 10 men and 14 women took part in that study. Previous studies showed a gender difference in PPI (Kumari. et al., 2004), but we evaluated only female subjects. We failed to detect any significant correlation between PPI and gray matter volume. The inconsistent results between previous studies and ours may be attributable, at least in part, to the fact that we examined only females who showed a narrow range of PPI. In conjunction with this, our study included only healthy women whose % PPI was changeable along with the menstrual cycle status (Swerdlow et al., 1997). Further studies work with information on menstrual cycle and studies on male subjects are necessary to address this issue.

In conclusion, the present study examined structural neural correlates of PPI and revealed evidence of a relationship between PPI and the integrity of white matter in healthy women. These observations confirm the involvement of these regions in human PPI as suggested by previous relevant data. Further research should extend the present methods in studies of clinical populations.

4.   Experimental procedures

4.1.   Sample

The subjects were 63 healthy females who were recruited from the community through local magazine advertisements and our website announcement. The participants were interviewed for enrollment using the Japanese version of the Mini-International Neuropsychiatric Interview (MINI) (Otsubo et al., 2005; Sheehan et al., 1998) by research psychiatrists, and only those who demonstrated no history of psychiatric illness or contact with psychiatric services were enrolled in the study. Participants were excluded if they had a prior medical history of central nervous system disease or severe head injury. In addition, 10 non-responders to the startle stimulus (see the "Prepulse inhibition measure" below) were also excluded from the analysis. As a consequence, 53 healthy females (mean age; 40.7 ± 11.3 years, education; 14.8 ± 2.7 years) took part in the study.

Written informed consent was obtained for participation in the study from all subjects, and the study was approved by the Ethics Committee of the National Center of Neurology and Psychiatry, Tokyo, Japan.

4.2.   Prepulse inhibition measure

Our equipment, setup, and standard PPI testing procedures have been described in detail (Kunugi et al., 2007). The startle reflex to acoustic stimuli was measured using the Startle Reflex Test Unit for Humans (O'Hara Medical, Tokyo). Subjects refrained from smoking for at least 20 min prior to the test. Broadband white noise (50 to 24,000 Hz) at 70 dB was presented as the background noise and was continuous throughout the session. Acoustic startle stimuli of the broadband white noise were presented through headphones.

During the initial 3 min of each session, the background noise alone was given for acclimation. In total, 35 startle-response trials were recorded in a session. These trials consisted of three blocks. In the first block, the subject's startle response to a pulse (sound pressure: 115 dB; duration: 40 ms) alone was recorded five times. In the second block, the subject's startle response to the same pulse with or without a prepulse (sound pressure: 86 or 90 dB; duration: 20 ms; lead interval [onset to onset]: 60 or 120 ms) was measured five times for each condition. The differential conditions of trials were presented in a pseudo-random order; however, the order was the same for all of the subjects. In the third and final block, the startle response to the pulse alone was again measured five times. The intertrial intervals (15 s on average, range 10 to 20 s) were randomly changed. The entire session lasted approximately 15 min. The mean % PPI of startle magnitude was calculated using the following formula, because in a previous study this condition showed the best sensitivity to differentiate between schizophrenic patients and healthy subjects (Kunugi et al., 2007):

% PPI=100 × (magnitude on pulse-alone trials−magnitude on prepulse trials {sound pressure: 86 dB and 90 dB; lead

interval: 120 ms, right eye})/magnitude on pulse-alone trials in the 2nd block.

The mean % PPI of the 53 subjects were 45.9±54.7 under the terms of 86 dB, and 58.8±39.8 of 90 dB. We defined a priori the "non-responders" to the startle stimuli as those subjects for whom the average value of the startle magnitude in the pulse-alone trials was <0.05 (digital unit), and the non-responders were excluded from the analysis.

4.3. MRI data acquisition

4.3.1. Data acquisition
MR imaging was performed on a Magnetom Symphony 1.5-T system (Siemens, Erlangen, Germany). High spatial resolution, 3-dimensional (3D) T1-weighted images of the brain were obtained for the morphometric study. The 3D T1-weighted images were scanned in the sagittal plane (echo time (TE)/repetition time (TR): 2.64/1580 ms; flip angle: 15°; effective slice thickness: 1.23 mm; slab thickness: 177 mm; matrix: 208 × 256; field of view (FOV): 256 × 315 mm^2; acquisition: (1), yielding 144 contiguous slices through the head.

DTI was performed in the axial plane (TE/TR: 106/11,200 ms; FOV: 240 × 240 mm^2; matrix: 96 × 96; 75 continuous transverse slices; slice thickness 2.5 mm with no interslice gap; acquisitions: (2). Diffusion was measured along 12 non-collinear directions with the use of a diffusion-weighted factor, b, in each direction for 1000 s/mm^2, and one image was acquired without use of a diffusion gradient. The DTI examination took approx. 6 min. In addition to DTI and 3D T1-weighted images, conventional axial T2-weighted images (TE/TR: 95/3500 ms; flip angle: 150°; slice thickness: 5 mm; intersection gap: 1.75 mm; matrix: 448 × 512; FOV: 210 × 240 mm^2; acquisitions: (1), and fluid attenuation inversion recovery (FLAIR) images in the axial plane (TE/TR: 101/8800 ms; flip angle: 150°; slice thickness: 3 mm; intersection gap: 1.75 mm; matrix: 448 × 512; FOV: 210 × 240 mm^2; acquisition: (1) were acquired to exclude cerebrovascular disease. On conventional MRI, no abnormal findings were detected in the brain in any subject.

4.3.2. Diffeomorphic anatomical registration using exponentiated lie analysis
The raw 3D T1-weighted volume data were transferred to a workstation. A preprocessing step of voxel-based morphometry (VBM) in Statistical Parametric Mapping (SPM) was improved with the DARTEL registration method (Ashburner, 2007). This technique, being more deformable, notably improves the realignment of small inner structures (Yassa and Stark, 2009). Calculations and image matrix manipulations were performed using SPM8 running on MATLAB R2007a software (MathWorks, Natick, MA). MR imaging data were analyzed using DARTEL as a toolbox for SPM8 to create a set of group-specific templates. The brain images were segmented, normalized, and modulated by using these templates. The output images were still in the average brain space. Additional warping from the Montreal Neurologic Institute space was given to the brain images. Then, gray matter probability values were smoothed by using an 8-mm full-width at half-maximum Gaussian kernel.

4.3.3. DTI procedure
The DTI data sets were analyzed using DtiStudio (Jiang et al., 2006). The diffusion tensor parameters were calculated on a pixel-by-pixel basis, and FA and MD map and $b=0$ image were calculated according to Wakana et al. (2004).

4.3.4. SPM analysis
To estimate the relationships between brain morphology and % PPI, FA and MD images were analyzed using an optimized VBM technique. The data were analyzed using SPM5 software running on MATLAB 7.0. The images were processed using an optimized VBM script. The details of this process are described elsewhere (Good et al., 2001). First, each individual 3D-T1 image was coregistered and resliced to its own $b=0$ image. Next, the coregistered 3D-T1 image was normalized to the "avg152T1" image regarded as the anatomically standard image in SPM5. Finally, the transformation matrix was applied to FA and MD maps. Further, to avoid the effect of diffusivity of cerebrospinal fluid (CSF), MD images were masked with the CSF image derived from the segmented individual 3D-T1 image. Each map was then spatially smoothed with a 6-mm full-width at half-maximum Gaussian kernel in order to decrease spatial noise and compensate for the inexactitude of normalization following the "rule of thumb" developed for fMRI and PET studies (Snook et al., 2007).

4.3.5. Tract-based spatial statistics (TBSS) analysis
The processing technique known as "tract-based spatial statistics (TBSS) analysis" projects DTI data onto a common pseudo-anatomical skeleton instead of trying to match each and every voxel in different subjects, and therefore does not need smoothing (Smith et al., 2006). TBSS is available as part of the FSL 4.1 software package (Smith et al., 2004). The TBSS script runs a nonlinear registration, aligning all FA images to the FMRIB58_FA template, which is supplied with FSL. The script then takes the target and affine-aligns it into a 1 × 1 × 1 mm MNI152 space. Once this is done, each subject's FA image has the nonlinear transform to the target and then the affine transform to MNI152 space is applied, resulting in a transformation of the original FA image into MNI152 space. Next, TBSS creates the mean of all aligned FA images and applies thinning of the local tract structure to create a skeletonized mean FA image. In order to exclude areas of low FA and/or high intersubject variability from a statistical analysis, TBSS thresholds a mean FA skeleton with a certain FA value, typically 0.2. The resulting binary skeleton mask is a pseudo-anatomical representation of the main fiber tracks, and defines the set of voxels used in all subsequent processing. Finally, TBSS projects each subject's aligned FA image onto the skeleton. This results in skeletonized FA data. It is this file that is used for the voxelwise statistics.

4.3.6. Statistical analysis
Statistical analyses were performed using SPM5 software (Welcome Department of Imaging Neuroscience, London, UK). Correlations between regional gray matter volume and % PPI with 86 and 90 dB of prepulse were assessed using the subjects' age, length of education, and whole brain volume as nuisance variables, and FA and MD value maps and % PPI

were assessed using age and education year as nuisance variables. Only correlations that met these criteria were deemed significant. In this case, a seed level of $p<0.001$ (uncorrected) and a cluster level of $p<0.05$ (uncorrected) were selected.

Skeletonized FA data were analyzed for revealing correlations with % PPI, controlling for age, using the FSL "Threshold-Free Cluster Enhancement (TFCE)" option in "randomise" with 5000 permutations, the script of which uses a permutation-based statistical inference that does not rely on a Gaussian distribution of voxels, and is run without having to define an initial cluster-forming threshold or carry out a large amount of data smoothing (Nichols and Holmes, 2002; Smith and Nichols, 2009). The significance level was set at the p-value of less than 0.05 with FWE rate correction for multiple comparisons.

Acknowledgments

REFERENCES

Ashburner, J., 2007. A fast diffeomorphic image registration algorithm. NeuroImage 38, 95–113.

Braff, D.L., Geyer, M.A., Swerdlow, N.R., 2001. Human studies of prepulse inhibition of startle: normal subjects, patient groups, and pharmacological studies. Psychopharmacology (Berl) 156, 234–258.

Cadenhead, K.S., Braff, D.L., 1999. Schizophrenia spectrum disorders. In: Dawson, M.E., Schell, A.M., Bohmelt, A.H. (Eds.), Startle Modification: Implications for Neuroscience. Cognitive Science, and Clinical Science. Cambridge University Press, Cambridge, pp. 231–244.

Fendt, M., Liang, L., Yeomans, J.S., 2001. Brain stem circuits mediating prepulse inhibition of the startle reflex. Psychopharmacology 156, 216–224.

Good, C.D., Johnsrude, I., Ashburner, J., Henson, R.N.A., Friston, K.J., Frackowiak, R.S.J., 2001. Cerebral asymmetry and the effect of sex and handedness on brain structure: a voxel-based morphometric analysis of 465 normal adult human brains. NeuroImage 14, 685–700.

Hazlett, E.A., Buchsbaum, M.S., Haznedar, M.M., Singer, M.B., Germans, M.K., Schnur, D.B., Jimenez, E.A., Buchsbaum, B.R., Troyer, B.T., 1998. Prefrontal cortex glucose metabolism and startle eyeblink modification abnormalities in unmedicated schizophrenia patients. Psychophysiology 35, 186–198.

Hazlett, E.A., Buchsbaum, M.S., Tang, C.Y., Fleischman, M.B., Wei, T.C., Byne, W., Haznedar, M.M., 2001. Thalamic activation during an attention-to-prepulse startle modification paradigm: a functional MRI study. Biol. Psychiatry 50, 281–291.

Hazlett, E.A., Buchsbaum, M.S., Zhang, J., Newmark, R.E., Glanton, C.F., Zelmanova, Y., Haznedar, M.M., Chu, K.W., Nenadic, I.,

Kemether, L.J., Tang, C.Y., New, A.S., Siever, L.J., 2008. Frontal–striatal–thalamic mediodorsal nucleus dysfunction in schizophrenia-spectrum patients during sensorimotor gating. NeuroImage 42, 1164–1177.

Jiang, H., van Zijil, P.C., Kim, J., Pearlson, G.D., Mori, S., 2006. DtiStudio: resource program for diffusion tensor computation and fiber bundle tracking. Comput. Methods Programs Biomed. 81, 106–116.

Koch, M, Schnitzler, H, 1997. The acoustic startle response in rats: circuits mediating evocation, inhibition and potentiation. Behav. Brain Res. 89, 35–49.

Kumari, V., Aasen, I., Sharma, T., 2004. Sex differences in prepulse inhibition deficits in chronic schizophrenia. Schizophr. Res. 69, 219–235.

Kumari, V., Antonova, E., Geyer, M.A., 2008a. Prepulse inhibition and "psychosis-proneness" in healthy individuals: an fMRI study. Eur. Psychiatry 23, 274–280.

Kumari, V., Antonova, E., Geyer, M.A., Ffytche, D., Williams, S.C., Sharma, T., 2007. A fMRI investigation of startle gating deficits in schizophrenia patients treated with typical or atypical antipsychotics. Int. J. Neuropsychopharmacol. 10, 463–477.

Kumari, V., Antonova, E., Zachariah, E., Galea, A., Aasen, I., Ettinger, U., Mitterschiffthaler, M.T., Sharma, T., 2005. Structural brain correlates of prepulse inhibition of the acoustic startle response in healthy humans. NeuroImage 26, 1052–1058.

Kumari, V., Fannon, D., Geyer, M.A., Premkumar, P., Antonova, E., Simmons, A., Kuipers, E., 2008b. Cortical grey matter volume and sensorimotor gating in schizophrenia. Cortex 44, 1206–1214.

Kumari, V., Gray, J.A., Geyer, M.A., Ffytche, D., Mitterschiffthaler, M.T., Vythelingum, G.N., Williams, S.C.R., Simmons, A., Sharma, T., 2003. Neural correlates of prepulse inhibition in normal and schizophrenic subjects: a functional MRI Study. Psychiatry Res.: NeuroImage 122, 99–113.

Kunugi, H., Tanaka, M., Hori, H., Hashimoto, R., Saitoh, O., Hironaka, N., 2007. Prepulse inhibition of acoustic startle in Japanese patients with chronic schizophrenia. Neurosci. Res. 59, 23–28.

McGhie, A, Chapman, J., 1961. Disorders of attention and perception in early schizophrenia. Br. J. Med. Psychol. 34, 103–116.

Moriwaki, M., Kishi, T., Takahashi, H., Hashimoto, R., Kawashima, K., Okochi, T., Kitajima, T., Furukawa, O., Fujita, K., Takeda, M., Iwata, N., 2009. Prepulse inhibition of the startle response with chronic schizophrenia: a replication study. Neurosci. Res. 65, 259–262.

Nichols, T.E., Holmes, A.P., 2002. Nonparametric permutation tests for functional neuroimaging: a primer with examples. Hum. Brain. Mapp. 15, 1–25.

Otsubo, T., Tanaka, K., Koda, R., Shinoda, J., Sano, N., Tanaka, S., Aoyama, H., Mimura, M., Kamijima, K., 2005. Reliability and validity of Japanese version of the Mini-International Neuropsychiatric Interview. Psychiatry Clin. Neurosci. 59, 517–526.

Perry, W., Minassian, A., Feifel, D., 2004. Prepulse inhibition in patients with non-psychotic major depressive disorder. J. Affect. Disord. 81, 179–184.

Sheehan, D.V., Lecrubier, Y., Sheehan, K.H., Amorim, P., Janavs, J., Weiller, E., Hergueta, T., Baker, R., Dunbar, G.C., 1998. The Mini-International Neuropsychiatric Interview (M.I.N.I.): the development and validation of a structured diagnostic psychiatric interview for DSM-IV and ICD-10. J. Clin. Psychiatry 59, 22–57.

Smith, S.M., Jenkinson, M., Johansen-Berg, H., Rueckert, D., Nichols, T.E., Mackay, C.E., Watkins, K.E., Ciccarelli, O., Cader, M.Z., Matthews, P.M., Behrens, T.E., 2006. Tract-based

spatial statistics: voxelwise analysis of multi-subject diffusion data. NeuroImage 31, 1487–1505.

Smith, S.M., Jenkinson, M., Woolrich, M.W., Beckmann, C.F., Behrens, T.E., Johansen-Berg, H., Bannister, P.R., De Luca, M., Drobnjak, I., Flitney, D.E., Niazy, R.K., Saunders, J., Vickers, J., Zhang, Y., De Stefano, N., Brady, J.M., Matthews, P.M., 2004. Advances in functional and structural MR image analysis and implementation as FSL. NeuroImage 23 (1), S208–219.

Smith, S.M., Nichols, T.E., 2009. Threshold-free cluster enhancement: addressing problems of smoothing, threshold dependence and localisation in cluster inference. NeuroImage 44, 83–98.

Snook, L., Plewes, C., Beaulieu, C., 2007. Voxel based versus region of interest analysis in diffusion tensor imaging of neurodevelopment. NeuroImage 34, 243–252.

Swerdlow, N.R., Geyer, M.A., 1998. Using an animal model of deficient sensorimotor gating to study the pathophysiology and new treatments of schizophrenia. Schizophrenia Bull. 24, 285–301.

Swerdlow, N.R., Geyer, M.A., Braff, D.L., 2001. Neural circuit regulation of prepulse inhibition of startle in the rat: current knowledge and future challenges. Psychopharmacology 156, 194–215.

Swerdlow, N.R., Hartman, P.L., Auerbach, P.P., 1997. Changes in sensorimotor inhibition across the menstrual cycle: implications for neuropsychiatric disorders. Biol. Psychiatry 41, 452–460.

Swerdlow, N.R., Weber, M., Qu, Y., Light, G.A., Braff, D.L., 2008. Realistic expectations of prepulse inhibition in translational models for schizophrenia research. Psychopharmacology (Berl) 199, 331–388.

Takahashi, H., Iwase, M., Ishii, R., Ohi, K., Fukumoto, M., Azechi, M., Ikezawa, K., Kurimoto, R., Canuet, L., Nakahachi, T., Iike, N., Tagami, S., Morihara, T., Okochi, M., Tanaka, T., Kazui, H, Yoshida, T, Tanimukai, H, Yasuda, Y, Kudo, T, Hashimoto, R, Takeda, M., 2008. Impaired prepulse inhibition and habituation of acoustic startle response in Japanese patients with schizophrenia. Neurosci. Res. 62, 187–194.

Wakana, S., Jiang, H., Nagae-Poetscher, L.M., van Zijl, P.C., Mori, S., 2004. Fiber tract-based atlas of human white matter anatomy. Radiology 230, 77–87.

Yassa, M.A., Stark, C.E., 2009. A quantitative evaluation of cross-participant registration techniques for MRI studies of the medial temporal lobe. NeuroImage 44, 319–327.

Immunohistochemical characterization of γ-secretase activating protein expression in Alzheimer's disease brains

J. Satoh*, H. Tabunoki*, T. Ishida†, Y. Saito‡ and K. Arima§

*Department of Bioinformatics and Molecular Neuropathology, Meiji Pharmaceutical University, Tokyo, †Department of Pathology and Laboratory Medicine, Kohnodai Hospital, NCGM, Chiba, ‡Department of Laboratory Medicine, National Center Hospital, NCNP, Tokyo, and §Department of Psychiatry, National Center Hospital, NCNP, Tokyo, Japan

---

J. Satoh, H. Tabunoki, T. Ishida, Y. Saito and K. Arima (2012) *Neuropathology and Applied Neurobiology* **38**, 132–141
Immunohistochemical characterization of γ-secretase activating protein expression in Alzheimer's disease brains

Aims: A recent study showed that γ-secretase activating protein (GSAP), derived from a C-terminal fragment of pigeon homolog (PION), increases amyloid-β (Aβ) production by interacting with presenilin-1 (PS1) and the β-secretase-cleaved C-terminal fragment of amyloid precursor protein (APP-CTF). In the study, knockdown of GSAP reduces production of Aβ and plaque formation in the brain of APPswe and PS1ΔE9 double transgenic mice without affecting the Notch-dependent pathway. Therefore, GSAP is an ideal target for designing γ-secretase modulators with least side effects in Alzheimer's disease (AD). However, at present, the precise distribution of GSAP in AD brains remains to be characterized. **Methods:** By immunohistochemistry, we studied GSAP expression in the frontal cortex and the hippocampus of 11 aged AD and 17 age-matched control cases. **Results:** GSAP immu- noreactivity exhibited distinct morphological features, such as fine granular cytoplasmic deposits, dense nodular and patchy deposits, beads and string-like deposits, and diffuse dot-like deposits. In both AD and control brains, a fairly small subset of cerebral cortical and hippocampal neurones expressed fine granular cytoplasmic deposits, while diffuse dot-like deposits were more frequently found in the neuropil and neuronal processes, particularly enriched in the hippocampal CA2 and CA3 regions. Among GSAP-immunoreactive deposits, dense nodular and patchy deposits, located in the neuropil and closely associated with PS1 expression and Aβ deposition, indi- cated the most distinguishing features of AD pathology. **Conclusions:** Aberrant regulation of GSAP expression plays a key role in acceleration of γ-cleavage of APP-CTF and accumulation of Aβ in AD brains.

Keywords: Alzheimer's disease, amyloid-β, GSAP, immunohistochemistry, PION

Introduction

Alzheimer's disease (AD) is the most common cause of dementia worldwide, affecting the elderly population,

Correspondence: Jun-ichi Satoh, Department of Bioinformatics and Molecular Neuropathology, Meiji Pharmaceutical University, 2-522-1 Noshio, Kiyose, Tokyo 204-8588, Japan. Tel: +81 42 495 8678; Fax: +81 42 495 8678; E-mail: satoj@my-pharm.ac.jp

The authors declare that there is no conflict of interest.

characterized by the hallmark pathology of widespread amyloid-β (Aβ) deposition and neurofibrillary tangle (NFT) formation in the brain [1]. The major amy- loidogenic peptides Aβ40/Aβ42 are generated by the consecutive cleavage of the amyloid precursor protein (APP) by β-secretase and γ-secretase. The latter forms a complex composed of presenilin-1 (PS1), anterior pharynx defective 1 homolog (APH1), presenilin enhancer 2 homolog (PEN2) and nicastrin. The presenilin complex regulates intramembrane proteolysis not only of

132

the β-secretase-cleaved C-terminal fragment of APP (APP-CTF) but also of Notch and cadherins, both of which play a pivotal role in transducing biologically essential signals [2]. Development of γ-secretase inhibitors and modulators that reduce Aβ production but do not affect the cleavage of other γ-secretase substrates is the most desirable approach for AD therapy to minimize toxic side effects of these drugs [3].

A previous study showed that an anticancer drug imatinib, named Gleevec, acts as a γ-secretase modulator that reduces production of Aβ38, Aβ40 and Aβ42 by inhibiting γ-cleavage of APP-CTF without affecting Notch processing [4]. Recently, the same group identified a γ-secretase activating protein (GSAP) that facilitates Aβ production by interacting with PS1-CTF and the juxtamembrane region of APP-CTF [5]. They found that GSAP is derived from a C-terminal fragment spanning amino acid residues 733-854 of pigeon homolog (PION), a protein of unknown biological function expressed in various tissues, including the brain. When expressed in cultured cells, the full-length human PION protein is rapidly cleaved, processed into GSAP via an unknown mechanism, and is accumulated in a trans-Golgi network. GSAP modulates γ-cleavage of APP but not of Notch. However, it differentially regulates γ-cleavage and ε-cleavage of APP-CTF. GSAP elevates the levels of Aβ derived from γ-cleavage, whereas it reduces the amount of the APP intracellular domain produced by ε-cleavage. Most importantly, knockdown of GSAP reduces production of Aβ and plaque formation in the brain of APPswe and PS1ΔE9 double transgenic mice without affecting the Notch-dependent pathway [5]. Imatinib actually achieves its Aβ-lowering effect by interfering with GSAP interaction with APP-CTF [5]. Thus, GSAP would represent an ideal target for designing γ-secretase modulators with least side effects for AD therapy [6].

However, at present, the precise distribution of GSAP in AD brains remains unknown. In the present study, we have attempted to characterize GSAP expression in AD brains by immunohistochemistry.

Materials and methods

Human brain tissues

Ten micron-thick serial sections of the hippocampus and the frontal cortex were prepared from autopsied brains of 11 AD patients, composed of five men and six women with

the mean age of 71 ± 9 years, and 17 non-AD patients, composed of 10 men and seven women with the mean age of 67 ± 8 years. The non-AD group includes four normal subjects died of non-neurological causes, four patients with myotonic dystrophy, three with Parkinson's disease, two with multiple system atrophy and four with amyotrophic lateral sclerosis. All AD cases were satisfied with the Consortium to Establish a Registry for Alzheimer's Disease criteria for diagnosis of definite AD [7]. Detailed characteristics of the brains employed are shown in Table S1, and were in part described previously [8–10]. All AD brains were categorized into the stage C of amyloid deposition and the stage VI of neurofibrillary degeneration, following the Braak staging system [11,12]. Autopsies on all subjects were performed at the National Center Hospital, National Center of Neurology and Psychiatry, Japan or Kohnodai Hospital, National Center for Global Health and Medicine, Japan. The pathological diagnosis was validated by comprehensive examination of autopsied brains by three established neuropathologists (K. A., Y. S., T. I.). Written informed consent was obtained from all the cases. The Ethics Committee of the corresponding institutions approved the present study.

Immunohistochemistry

The brain tissues were fixed with 4% paraformaldehyde and embedded in paraffin. After deparaffinization, tissue sections were heat-treated in 10 mM citrate sodium buffer, pH 6.0 by autoclaving them at 125°C for 30 s in a temperature-controlled pressure chamber (Dako, Tokyo, Japan). For Aβ immunolabelling, they were pretreated with formic acid for 5 min at room temperature (RT). The tissue sections were exposed at RT for 15 min to 3% hydrogen peroxide-containing methanol to block the endogenous peroxidase activity. They were then incubated with phosphate-buffered saline (PBS) containing 10% normal goat serum at RT for 15 min to block non-specific staining. Subsequently, they were incubated in a moist chamber at 4°C overnight with a rabbit anti-GSAP antibody raised against the peptide spanning amino acid residues 769-840 of the human PION protein, composed of HPMSSNI ISRNHVTRLLQNYKKQPRNSMINKSSFSVEFLPLNYFIEIL TDIESSNQALYPFEGHDNVDAEFV (1:100, HPA020058; Sigma, St. Louis, MO, USA) or a rabbit anti-PION non-GSAP fragment antibody raised against the peptide spanning amino acid residues 471-558 of the human PION protein, composed of SSYWSVYSETSNMDKLLPHSSVLT